

DOKUZ EYLÜL UNIVERSITY
GRADUATE SCHOOL OF NATURAL AND APPLIED SCIENCES

**THE ELECTRICAL AND THERMAL
BREAKDOWN OF THE INTEGER
QUANTIZED HALL EFFECT:
A MICROSCOPIC
SELF-CONSISTENT INVESTIGATION**

by

Nazlı BOZ YURDAŞAN

February, 2012

İZMİR

**THE ELECTRICAL AND THERMAL
BREAKDOWN OF THE INTEGER
QUANTIZED HALL EFFECT:
A MICROSCOPIC
SELF-CONSISTENT INVESTIGATION**

**A Thesis Submitted to the
Graduate School of Natural and Applied Sciences of Dokuz Eylül University
In Partial Fulfillment of the Requirements for the Degree
of Doctor of Philosophy in
Physics**

by

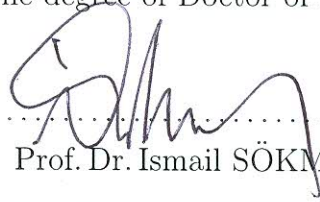
Nazlı BOZ YURDAŞAN

February, 2012

İZMİR

Ph.D. THESIS EXAMINATION RESULT FORM

We have read the thesis entitled “**THE ELECTRICAL AND THERMAL BREAKDOWN OF THE INTEGER QUANTUM HALL EFFECT: A MICROSCOPIC SELF-CONSISTENT INVESTIGATION**” completed by **NAZLI BOZ YURDAŞAN** under supervision of **PROF. DR. İSMAİL SÖKMEN** and we certify that in our opinion it is fully adequate, in scope and in quality, as a thesis for the degree of Doctor of Philosophy.


.....
Prof. Dr. Ismail SÖKMEN

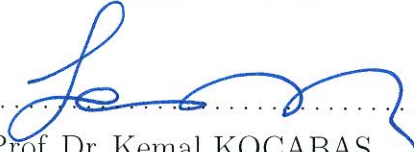
Supervisor


.....
Prof. Dr. Müriyyet YURDAKOÇ


Thesis Committee Member


.....
Assist. Prof. Dr. Kadir AKGÜNGÖR

Thesis Committee Member


.....
Prof. Dr. Kemal KOCABAŞ

Examining Committee Member


.....
Assoc. Prof. Dr. Afif SİDDİKİ

Examining Committee Member


.....
Prof. Dr. Hamza POLAT

Examining Committee Member


.....
Assist. Prof. Dr. Uğur ERKASLAN

Examining Committee Member


.....
Prof. Dr. Mustafa SABUNCU

Director Graduate School of Natural and Applied Sciences

ACKNOWLEDGEMENTS

I would like to express my gratitude to all those who gave me the possibility to complete my Ph.D. study.

I owe my most deep and sincere gratitude to my supervisor Prof. Dr. İsmail SÖKMEN for the continuous support of my Ph.D study and research, for his endless patience, motivation, understanding, advise and immense knowledge. His wide knowledge and logical way of thinking have been of great guidance for me.

I would like to express my sincere gratitude to my second supervisor Assoc. Prof. Dr. Afif SİDDİKİ for giving me the opportunity to work in this subject and in his group 'Nano-electronic and Nano-transport'. His guidance and critical comments help me in all the time of research and writing of this thesis.

I am very grateful to Prof. Dr. R. R. GERHARDTS for sharing with me his Fortran codes and his constructive comments.

My sincere thanks also goes to Asist. Prof. Dr. Kadir AKGÜNGÖR for spending his time even for answering my questions. Also his technical support contributes to this thesis.

I wish to thank my all friends for helping me get through the difficult times, for all the emotional support and entertainment.

Finally, I owe so much thanks to my parents, Zühra-Nusret BOZ who are continuously supporting me throughout my life. I would like to extend a very special thanks to my husband Fatih YURDAŞAN for his understanding and love, for making my mind relax during the hard times. I also would like to thank to my son, Metehan YURDAŞAN for giving me unlimited happiness and pleasure.

Nazlı BOZ YURDAŞAN

THE ELECTRICAL AND THERMAL BREAKDOWN OF THE INTEGER QUANTIZED HALL EFFECT: A MICROSCOPIC SELF-CONSISTENT INVESTIGATION

ABSTRACT

In this thesis, spatial distributions of the electron temperature were investigated employing thermohydrodynamic theory in quantum Hall effect observed in two dimensional electron systems subjected to low temperatures and strong magnetic fields. This theory was described by equations of conservation with number and thermal flux densities.

In the linear-response regime, spatial distributions of the electron temperature related to the incompressible strips were calculated. The importance of the electron temperature was shown in various phenomena, such as breakdown of the quantum Hall effect. After calculating the electron temperature, the effects of the electron temperature deviation on distributions of the current density were discussed.

In the second part of the thesis, the changes of the incompressible strips with the deviation of the electron temperature from the lattice temperature were presented. Position dependencies of the electrostatic potential and electron density were calculated with the electron temperature using the self-consistent Thomas-Fermi-Poisson approximation. Also electrochemical potential and current density were obtained from a local version of Ohm's law. These results were compared with those obtained by the lattice temperature.

Keywords: Quantum Hall effect, linear-response regime, thermohydrodynamics theory, local equilibrium.

TAMSAYILI KUANTİZE HALL ETKİSİNİN ELEKTRİKSEL VE TERMAL KIRILMASININ MİKROSKOPİK ÖZUYUMLU OLARAK İNCELENMESİ

ÖZ

Bu tezde, düşük sıcaklıklara ve güçlü manyetik alanlara bağlı iki boyutlu elektron sistemlerinde gözlenen kuantum Hall etkisindeki termohidrodinamik teori uygulanarak elektron sıcaklığının uzaysal dağılımı incelendi. Bu teori sayı ve termal akı yoğunluğu denklemleri ile tanımlandı.

Lineer-tepki sistemi altında, sıkıştırılmaz şeritlere bağlı elektron sıcaklığının uzaysal dağılımı hesaplandı. Elektron sıcaklığının önemi, kuantum Hall etkisinin kırılması gibi çeşitli fenomenlerde gösterildi. Elektron sıcaklığının hesaplanmasından sonra, elektron sıcaklık değişiminin akım yoğunluğu üzerindeki etkileri tartışıldı.

Tezin ikinci kısmında, elektron sıcaklığının örgü sıcaklığından sapmasıyla sıkıştırılmaz şeritlerin değişimleri sunuldu. Elektrostatik potansiyelin ve elektron yoğunluğunun konuma bağımlılıkları, öz-uyumlu Thomas-Fermi-Poisson yaklaşımı kullanılarak elektron sıcaklığı altında hesaplandı. Ayrıca elektrokimyasal potansiyel ve akım yoğunluğu yerel Ohm yasası ile bulundu. Bu sonuçlar örgü sıcaklığından elde edilen sonuçlarla karşılaştırıldı.

Anahtar sözcükler: Kuantum Hall etkisi, lineer-tepki sistemi, termohidrodinamik teori, yerel denge.

CONTENTS

| | Page |
|--|-------------|
| Ph.D. THESIS EXAMINATION RESULT FORM | ii |
| ACKNOWLEDGEMENTS | iii |
| ABSTRACT | iv |
| ÖZ | v |
| CHAPTER ONE - INTRODUCTION | 1 |
| CHAPTER TWO - TWO DIMENSIONAL ELECTRON SYSTEM AND THE QUANTUM HALL EFFECT | 4 |
| 2.1 Two Dimensional Electron System (2DES) | 4 |
| 2.2 The Physical System | 6 |
| 2.3 Magnetotransport in the Classical Regime | 7 |
| 2.4 Landau Level Quantization in High Magnetic Fields | 10 |
| 2.5 Magnetotransport in the Quantum Regime | 12 |
| 2.5.1 Integer Quantum Hall Effect (IQHE) | 13 |
| 2.5.2 Localized and Extended States | 14 |
| 2.5.3 Excitation and Relaxation of Hot Electrons..... | 16 |
| 2.5.4 Breakdown of the QHE | 17 |
| CHAPTER THREE-FUNDAMENTALS OF THE SCREENING THEORY . | 21 |
| 3.1 Introduction..... | 21 |
| 3.2 Thermal Equilibrium..... | 21 |
| 3.3 Local Equilibrium with Imposed Current..... | 23 |
| 3.4 Result: Lattice Temperature at Position Independent Electron Temperature | 24 |
| CHAPTER FOUR-THERMOHYDRODYNAMIC THEORY IN QUANTUM HALL SYSTEMS | 28 |

| | | |
|---|---|-----------|
| 4.1 | Introduction..... | 28 |
| 4.2 | Model, Processes and Macroscopic Variables | 28 |
| 4.2.1 | Drift and Hopping Processes | 28 |
| 4.2.2 | Model | 28 |
| 4.2.3 | Macroscopic Variables | 29 |
| 4.3 | Thermo-hydrodynamical Equations | 29 |
| 4.3.1 | Hopping Components of the Total Flux Densities..... | 31 |
| 4.3.1.1 | The Number Flux Density..... | 31 |
| 4.3.1.2 | The Thermal Flux Density | 33 |
| 4.3.2 | Drift Components of the Total Flux Densities | 34 |
| 4.3.3 | Total Flux Densities | 39 |
| 4.3.4 | Transport Coefficients..... | 40 |
| 4.3.5 | Boundary Conditions and Edge Current | 40 |
| 4.3.6 | Energy Loss | 43 |
| CHAPTER FIVE-POSITION DEPENDENT ELECTRON TEMPERATURE IN LINEAR RESPONSE REGIME - RESULTS | | 45 |
| 5.1 | Introduction..... | 45 |
| 5.2 | Electron Temperature and Current Density | 46 |
| 5.2.1 | Lattice Temperature Dependence..... | 46 |
| 5.2.2 | Magnetic Field Dependence | 51 |
| 5.2.3 | Sample Parameter Dependence | 54 |
| 5.3 | Effects of the Energy Loss on the Electron Temperature..... | 56 |
| 5.4 | Effects of the Electron Temperature on the Compressible and the Incompressible Strips | 58 |
| CHAPTER SIX - TEMPERATURE DEPENDENT BREAKDOWN OF THE QUANTUM HALL RESISTANCE | | 64 |
| 6.1 | Introduction..... | 64 |
| 6.2 | Model and Results | 65 |
| 6.3 | Conclusion..... | 68 |

| | |
|---|-----------|
| CHAPTER SEVEN - CONCLUSION | 70 |
| REFERENCES | 73 |
| APPENDIX A | 79 |
| A.1 Background (Free Electron Theory of Metals) | 79 |
| A.1.1 Drude model | 79 |
| A.1.2 Electrical conductivity | 79 |
| A.1.3 Thermal conductivity | 81 |
| A.2 Wiedemann-Franz law | 82 |
| A.3 Thermoelectric Cooling and Heating..... | 83 |
| A.4 Fermi Dirac Distribution Function | 84 |
| A.5 Thermodynamic Potential | 85 |
| APPENDIX B | 87 |
| B.6 Density of States with Magnetic Field | 87 |
| ABBREVIATIONS and SYMBOLS | 90 |

CHAPTER ONE

INTRODUCTION

The Hall Effect was discovered by Edwin Herbert Hall in 1879 while working on his doctoral degree at Johns Hopkins University in Maryland, USA. The Hall effect is the production of a voltage difference, which is called the Hall voltage, across an electrical conductor, transverse to an electric current in the conductor and a magnetic field perpendicular to the current (Hall, 1879). The discovery of Quantum Hall Effect (QHE) by Klaus von Klitzing in 1980 is a remarkable achievement in condensed matter physics. QHE is a striking set of phenomena which occur at low temperatures (≤ 4 K) in a high mobility two dimensional electron gas in a strong transverse magnetic field (typically, $B \sim 1 - 30$ T). The quantization was observed in the Hall resistance R_H , which exhibited plateaus at values of $R_H = h/ie^2$, where h is Planck's constant, e is the electron charge and i is an integer. This integer represents the number of completely filled Landau levels (LLs). The resistance quantum $R_K = h/e^2$ is named as the von Klitzing constant and corresponds to the value of 25812.807Ω (Klitzing, Dorda, & Pepper, 1980). In 1990, this resistance is accepted as an international resistance standard. For his discovery, von Klitzing was awarded the Nobel prize in physics in 1985 (Klitzing, 1986). In 1982 D.C.Tsui, H.L.Störmer, and A.C.Gossard discovered the existence of Hall steps with rational fractional quantum numbers, which is called the fractional QHE. R.B.Laughlin's wave functions established a very good, though not yet perfect understanding of this phenomenon. Today, the study of quasi particles of fractional charge and fractional statistics are still active areas of research (Tsui, Stormer, & Gossard, 1982; Stormer *et. al.*, 1983).

Most studies of the QHE have been performed on a two dimensional electron system (2DES) in a semiconducting device, realized with a Silicon metal-oxide semiconductor field-effect transistor (MOSFET) at liquid Helium temperatures and high magnetic fields (Klitzing, Dorda, & Pepper, 1980). The QHE is studied by analyzing the electrical breakdown, the time resolved transport, the edge channels and the behavior of composite fermions. The 2DES resides, primarily, in a narrow potential well

(inversion layer) near the interface by the electrostatic attraction to a positively charged layer somewhere away from the interface in the other material. The first measurements performed with Si-MOSFETs were done by Fowler et al. in 1966. Although SiO₂-Si interface was used initially, then heterojunctions, especially (GaAs-Al_xGa_{1-x}As) heterojunctions, have come to be more widely used since they can be made with higher mobilities.

Shortly after the discovery of the QHE, experiments were performed to determine the physical limits of the effect (Ebert, Klitzing, Ploog, & Weimann, 1983). The sample temperature and the electrical current through the 2DES are important for the formation of the quantum Hall (QH) plateaus like electron density and electron mobility. The studies in QHE, if the temperature is increased, the longitudinal resistivity ρ_{xx} increases smoothly and the Hall resistivity ρ_{xy} deviates from the plateau values. When the sample current is small, ρ_{xx} is extremely in QHE which occurs. If the current is increased up to a critical value, ρ_{xx} increases by several orders of magnitude within a narrow range of the current, and the QHE breaks down (Ebert, Klitzing, Ploog, & Weimann, 1983; Cage et al., 1983; Kuchar, Bauer, Weimann, & Burkhard, 1984). On the other hand, theoretically, as a mechanism of the breakdown, a hot electron model (Ebert, Klitzing, Ploog, & Weimann, 1983; Komiyama, Takamasu, Hiyamizu, & Sasa, 1985) has been proposed, which assembles electron heating and the high electron temperature dependence of ρ_{xx} . Gurevich and Mints in 1984 have proposed a hydrodynamic equation based on the hot-electron model to calculate spatio-temporal variations of in quantum Hall systems (QHS) (Aker, & Suzuura, 2005).

In this thesis, spatial dependence of the electron temperature is investigated in QHS with the compressible and incompressible strips using the thermohydrodynamic theory in the linear response regime. Spatial variation of the electron temperature is taken into account in order to calculate the physical quantities, such as electron and current densities. This thesis is structured as follows:

- **Chapter 2:** contains the fundamentals of a 2DES formed in GaAs/AlGaAs heterostructures, which leads to the QHE through the Landau quantization in magnetotransport measurements. A description of the integer quantum Hall effect (IQHE) and the electrical breakdown of the IQHE is given.
- **Chapter 3:** introduces Thomas Fermi approximation for the self-consistent calculation. Typical results based on this approach are presented. In these calculations, the electron temperature is taken into account uniformly in QHS.
- **Chapter 4:** describes the investigated model, processes and macroscopic variables. Then, the thermohydrodynamic theory is determined using equations of conservation and thermal flux densities.
- **Chapter 5:** gives results of numerical calculations for spatial distribution of the electron temperature and current density depending on lattice temperature, magnetic field and sample parameters. The effect of a heat transfer due to the electron phonon scattering on the spatial variation of electron temperature is discussed. Then, influences of the electron temperature on the compressible and incompressible strips are obtained including the heat transfer.
- **Chapter 6:** includes Hall resistances within a local version of the Ohm's law and numerically investigate the dependencies of the overshoot on lattice temperature and magnetic field.
- **Chapter 7:** summarizes the present work.

CHAPTER TWO

TWO DIMENSIONAL ELECTRON SYSTEM AND THE QUANTUM HALL EFFECT

2.1 Two Dimensional Electron System (2DES)

The quantum Hall effect is closely related to technological advances in the fabrication of 2DES with high electronic mobilities. 2DES is formed at the interface of a heterostructure in which the electrons are completely confined in the potential well in the z -direction, however they are quasi free to move in the $x - y$ plane. Thus, the total energy is given by

$$E = E_z^0 + \frac{\hbar^2(k_x^2 + k_y^2)}{2m^*}, \quad (2.1.1)$$

where E_z^0 is energy of the first subband, k_x and k_y are the wave vector components in the momentum space and m^* is the effective electron mass. In the z -direction, the wave function of the electrons is localized in GaAs, since the potential well is quite asymmetric.

These systems are assembled of different materials. The first studies of the integer quantum Hall effect were performed using MOSFET. A metallic layer is separated from a semiconductor, typically silicon doped, by an insulating oxide such as SiO_2 layer (Klitzing, Dorda, & Pepper, 1980). A common heterostructure that is fabricated is shown in Figure 2.1(a). The system is grown on the GaAs substrate wafer, typically ~ 0.5 mm thick. A thick buffer layer of GaAs is grown on it to create a smooth surface and move the important layers away from the defects and impurities present on the wafer surface. On top of the substrate, a cleaning superlattice is grown consisting of ~ 100 alternating AlGaAs, followed by GaAs layers which getter and trap impurities at the GaAs/AlGaAs interfaces. Another thick GaAs layer is grown and then the GaAs/AlGaAs interface for the 2DES. The Si dopants are placed remotely from this interface (modulation doped). A layer of AlGaAs separates the 2DES from the sample surface. A thin cap of GaAs is grown on the surface to prevent oxidation of

the AlGaAs. This arrangement of the layers along vertical axis produces conduction band shown on Figure 2.1(b).

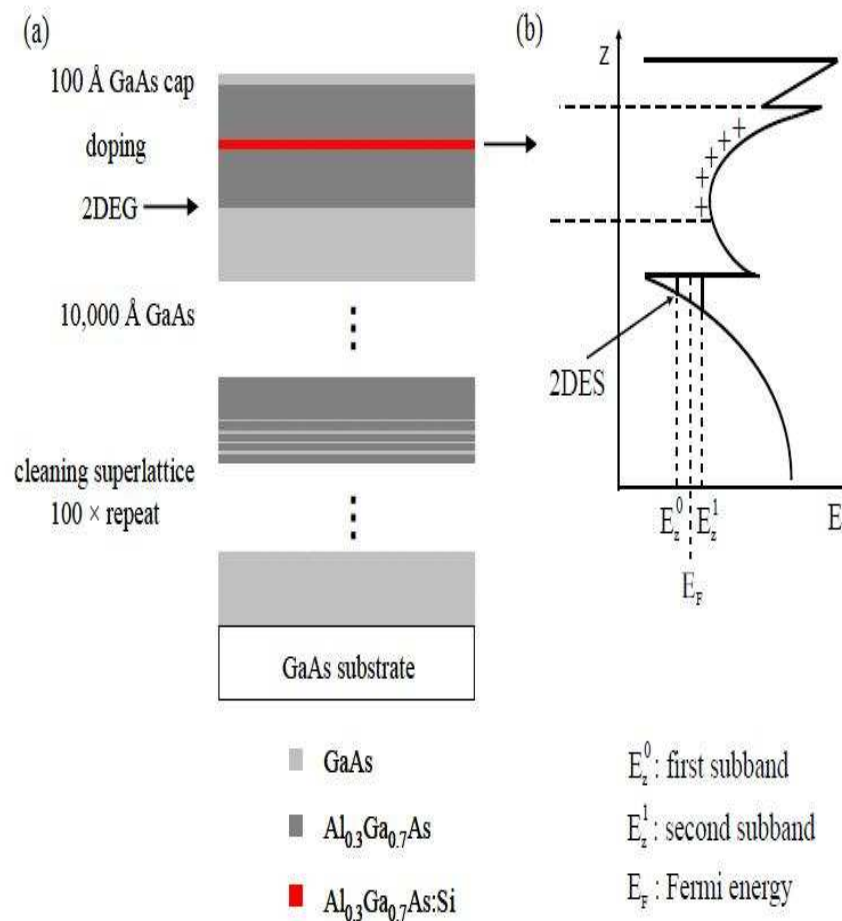


Figure 2.1 (a) A typical modulation doped GaAs/AlGaAs heterostructure and (b) its conduction band.

If the Schrödinger and the Poisson equations are solved self-consistently to obtain the energy band diagram of the structure, then a triangular potential well occurs at the heterojunctions and its thickness is equal or smaller than the de Broglie wavelength of the electrons.

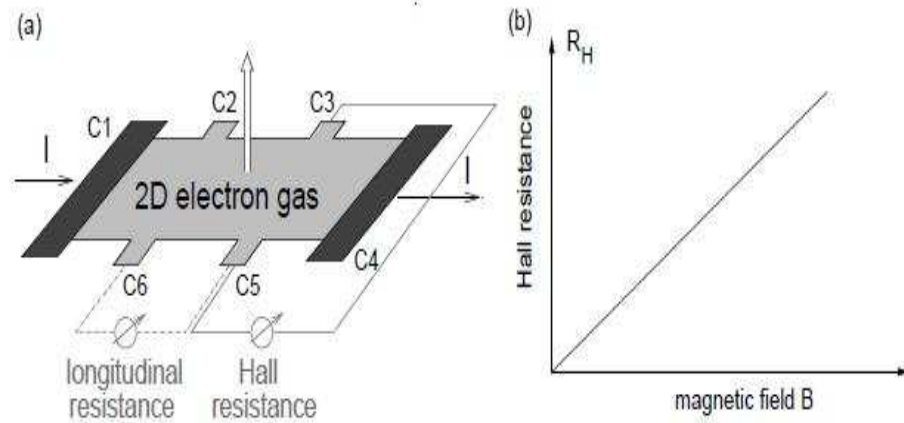


Figure 2.2 (a) 2D electrons in a perpendicular magnetic field (QHS). (b) Classical Hall resistance as a function of the magnetic field.

2.2 The Physical System

The quantum Hall effect occurs in two-dimensional electron systems in the limit of strong perpendicular magnetic fields at very low temperatures. These systems do not occur naturally, but it has become possible to produce them by using advanced technology and production techniques developed within semiconductor electronics.

To understand physical properties of a two dimensional electron gas in a perpendicular magnetic field, we consider the Hall bar geometry shown in Figure 2.2 (a). There is six ohmic contacts, which are contacted to the 2DES. An electric field E_x applied between C1 and C4 contacts causes an electric current I flowing in the Hall bar. A longitudinal voltage V_L is measured between C5 and C6 contacts and a Hall voltage V_H is measured between C3 and C6 contacts. However, when a perpendicular magnetic field is applied, electrons accumulate on one edge of the Hall bar. This leaves equal and opposite charges exposed on the opposite edges until the transverse electric force $\mathbf{F}_E = -e\mathbf{E}$ becomes equal to Lorentz force $\mathbf{F}_L = -e(\mathbf{E} + \mathbf{v} \times \mathbf{B})$.

2.3 Magnetotransport in the Classical Regime

The first observation of the classical Hall effect has been carried out by E. H. Hall in 1879. He observed that when a metal plate (in the $x - y$ plane) is placed in a perpendicular magnetic field, $\mathbf{B} = B\hat{z}$, and a current, I , is Hall effect in the driven in the x -direction as illustrated in Figure 2.2 (a). This effect is known as classical electromagnetism. After the imposition of a current along the x -direction he observed a longitudinal resistance independent of the magnetic field and a transverse voltage which defines a transverse resistance, known as Hall resistance, linear in magnetic field through the relation Figure 2.2 (b),

$$R_H = \frac{B}{n_{\text{el}}q}, \quad (2.3.1)$$

with n_{el} the electron density and q the carrier charge. The Drude model is applied for diffusive transport in a metal to explain the experimental observation (Ashcroft, & Mermin, 1984; Kittel, 1953).

The two dimensional motion of N free electrons are considered in the xy plane subjected to a perpendicular magnetic field in z -direction, which is homogeneous along the plane, i.e. independent of x and y directions. The free electron system dimensions are L_x and L_y along the x and y directions respectively. So the two dimensional electron density is given by

$$n_{\text{el}} = \frac{N}{L_x L_y}. \quad (2.3.2)$$

After the electric field is applied, the drift velocity of the electrons is deflected in the y -direction because of the magnetic field. Therefore electrons accumulate on one edge of the Hall bar, and a positive ion excess is established on the opposite edge until the transverse electric force \mathbf{F}_E just cancels the Lorentz force \mathbf{F}_L due to the magnetic

field. In a uniform magnetic field \mathbf{B} the Lorentz force on an electron is

$$\mathbf{F}_L = -e[\mathbf{E} + \mathbf{v} \times \mathbf{B}], \quad (2.3.3)$$

where \mathbf{v} is the velocity of the electrons. In this equation, the first and second terms depend on the electric and magnetic fields respectively. The effect of scattering is introduced via a relaxation time τ . The Newtonian equation of motion for such a classical electron can be written as

$$m^* \left(\frac{d\mathbf{v}}{dt} + \frac{\mathbf{v}}{\tau} \right) = -e[\mathbf{E} + \mathbf{v} \times \mathbf{B}], \quad (2.3.4)$$

where $m^* d\mathbf{v}/dt$ is the free electron acceleration term and $m^* \mathbf{v}/\tau$ is the effect of collisions with τ . In steady state we get

$$m^* \frac{\mathbf{v}}{\tau} = -e[\mathbf{E} + \mathbf{v} \times \mathbf{B}]. \quad (2.3.5)$$

For the uniform electric field in the $x - y$ plane, $\mathbf{E} = (E_x, E_y, 0)$ and the magnetic field to be along the z -direction, $\mathbf{B} = (0, 0, B)$, $m^* \mathbf{v}/\tau$ term of the above equation can be written in matrix form as

$$\begin{pmatrix} E_x \\ E_y \end{pmatrix} = \begin{pmatrix} -m^*/e\tau & -B \\ B & -m^*/e\tau \end{pmatrix} \begin{pmatrix} v_x \\ v_y \end{pmatrix}. \quad (2.3.6)$$

The presence of this two components implies the existence of two different potentials with V_H for the transversal direction and V_L for the longitudinal direction of the Hall bar. These potential components can be written as

$$\begin{aligned} V_L &= E_x L_x, \\ V_H &= E_y L_y. \end{aligned} \quad (2.3.7)$$

In terms of the current following along the sample

$$I = J_x L_y, \quad (2.3.8)$$

they become

$$\begin{aligned} V_L &= \frac{m^*}{n_{e1} e^2 \tau} I \frac{L_x}{L_y}, \\ V_H &= -\frac{B}{n_{e1} e} I. \end{aligned} \quad (2.3.9)$$

The resistances are defined as

$$\begin{aligned} R_L &= \frac{V_L}{I} = \left(\frac{m^*}{n_{e1} e^2 \tau} \right) \frac{L_x}{L_y}, \\ R_H &= -\frac{V_H}{I} = \frac{B}{n_{e1} e}. \end{aligned} \quad (2.3.10)$$

As it is seen, R_L does not depend on the magnetic field \mathbf{B} , but R_H which is called the Hall resistance, increases linearly with magnetic field \mathbf{B} . This is called the classical Hall effect. This effect is seen in Figure 2.3 , where the classical Hall effect is observed between 0 and 0.4 T. The Hall effect is used as a conventional method to determine the electron concentration and the mobility of a 2DES by using the Equation 2.3.10. By introducing the current density

$$\mathbf{J} = -en_{e1}\mathbf{v}, \quad (2.3.11)$$

the conductivity tensor can be identified as

$$\boldsymbol{\sigma} = \begin{pmatrix} \sigma_{xx} & \sigma_{xy} \\ \sigma_{yx} & \sigma_{yy} \end{pmatrix} = \begin{pmatrix} \frac{n_{e1} e^2 \tau}{m^*} & -\frac{n_{e1} e}{B} \\ \frac{n_{e1} e}{B} & \frac{n_{e1} e^2 \tau}{m^*} \end{pmatrix} \quad (2.3.12)$$

$$= \frac{\sigma_0}{1 + (\omega_c \tau)^2} \begin{pmatrix} 1 & -\omega_c \tau \\ \omega_c \tau & 1 \end{pmatrix}. \quad (2.3.13)$$

where $\sigma_0 = n_{\text{el}}e^2\tau/m^*$ is the classical Drude conductivity and eB/m^* is the cyclotron frequency. From the above equation it is clear that $\sigma_{xx} = \sigma_{yy}$ and $\sigma_{xy} = -\sigma_{yx}$. The resistivity tensor is the inverse of the conductivity tensor $\hat{\rho} = \hat{\sigma}^{-1}$ and written as

$$\rho = \begin{pmatrix} \rho_{xx} & \rho_{xy} \\ \rho_{yx} & \rho_{yy} \end{pmatrix} = \frac{1}{\sigma_{xx}^2 + \sigma_{xy}^2} \begin{pmatrix} \sigma_{xx} & -\sigma_{xy} \\ \sigma_{xy} & \sigma_{xx} \end{pmatrix}, \quad (2.3.14)$$

$$= \rho_0 \begin{pmatrix} 1 & \omega_c \tau \\ -\omega_c \tau & 1 \end{pmatrix}, \quad (2.3.15)$$

with $\rho_0 = 1/\sigma_0$ the resistivity tensor components obey the same Onsager symmetry relations, such that $\rho_{xx} = \rho_{yy}$ and $\sigma_{xy} = -\sigma_{yx}$. From this tensor relation the longitudinal and the transverse resistivity components are given by

$$\begin{aligned} \rho_{xx} &= \frac{1}{n_{\text{el}}e\mu}, \\ \rho_{xy} &= \frac{B}{n_{\text{el}}e}, \end{aligned} \quad (2.3.16)$$

where $\mu = e\tau/m^*$ is the mobility which determines the quality of the 2DES.

2.4 Landau Level Quantization in High Magnetic Fields

The origins of the quantum Hall effect can be only found by quantum mechanical calculations. For this, a starting point is Schrödinger equation for an electron in a constant magnetic field:

$$\left[\frac{1}{2m^*} (\hat{\mathbf{p}} + e\mathbf{A})^2 + eV(x, y) \right] \Psi(x, y) = \varepsilon \Psi(x, y). \quad (2.4.1)$$

In this equation the electron-electron interaction and the spin are neglected. The magnetic field is applied in z -direction and Landau gauge is used for the vector potential $\mathbf{A} = (-By, 0, 0) = -B_y \hat{i}$. This gauge is appropriate for systems with translational sym-

metry along y axis. If the external potential is assumed to vanish ($V(x, y) = 0$, no electric field) and Landau gauge symmetry is introduced, the Schrödinger equation is rewritten as

$$\frac{1}{2m^*} [(\hat{p}_x - eB_y)^2 + \hat{p}_y^2] \Psi(x, y) = \varepsilon \Psi(x, y). \quad (2.4.2)$$

The operator \hat{p}_x commutes with the Hamiltonian ($[\hat{H}, \hat{p}_x] = 0$) and the problem separates into two independent subspaces for x and y . The operator \hat{p}_x and \hat{p}_y in the x and y subspace are expressed by $\hat{p}_x = -i\hbar\partial/\partial x$ and $\hat{p}_y = -i\hbar\partial/\partial y$. The wave function $\Psi(x, y)$ is written as

$$\Psi(x, y) = \phi_n(y) \exp(ikx). \quad (2.4.3)$$

Then substituting the wave function in Equation 2.4.1, Schrödinger equation is rewritten as

$$\frac{1}{2m^*} [(\hbar k_x - eB_y)^2 - \hbar^2 \partial^2/\partial y^2] \phi_n(y) = \varepsilon_n \phi_n(y). \quad (2.4.4)$$

This equation describes an effective one dimensional harmonic oscillator

$$\left[-\frac{\hbar^2}{2m^*} \frac{\partial^2}{\partial y^2} + \frac{1}{2} m^* \omega_c^2 (y - Y)^2 \right] \phi_n(y) = \varepsilon_n \phi_n, \quad (2.4.5)$$

with a cyclotron frequency $\omega_c = eB/(m^*)$ and a center coordinate $Y = -l^2 k_y$. Here $l = \sqrt{\hbar/eB}$ is the magnetic length, depending only on the magnetic field B . The eigenvalues ε_n of this harmonic oscillator is

$$\varepsilon_n = \hbar \omega_c \left(n + \frac{1}{2} \right), \quad n = 0, 1, 2, \dots \quad (2.4.6)$$

The energy eigenvalues are called Landau levels. This equation shows how 2DES energy spectrum is quantized due to the magnetic field. From the quantization of the energy spectrum, density of states (DOS) that is constant at zero magnetic field, becomes discretized at high magnetic field

$$D(\varepsilon) = n_L \sum_{n,s} \delta(\varepsilon - \varepsilon_{n,s}). \quad (2.4.7)$$

Here n_L is number of the electrons in each Landau level given by

$$n_L = 2 \frac{eB}{h} \quad (\text{without spin splitting}). \quad (2.4.8)$$

This is also called the degeneracy factor of the Landau levels, which is independent of the semiconductor parameters such as effective mass. If the spin splitting is taken into account, the degeneracy of a spin split Landau level becomes

$$n_L = \frac{eB}{h}. \quad (2.4.9)$$

This is called filling factor and gives the number of filled Landau levels

$$\nu = \frac{n_{el}}{n_L} = \frac{hn_{el}}{eB}. \quad (2.4.10)$$

2.5 Magnetotransport in the Quantum Regime

In the classical regime, we see the linear dependence of the Hall resistance R_H or Hall resistivity ρ_H on the strength of the magnetic field B at low magnetic fields where the number of filled Landau level's (LL) is larger. If the magnetic field is increased the magnetic field and LL's are reduced, the Hall resistance or Hall resistivity shows a different behavior that is given in Figure 2.3. This figure shows a typical magnetotransport curve with its three important regimes. The first regime is the classical that is seen at low magnetic fields, up to 0.4 T for this sample. The Hall resistivity increases linearly with the magnetic field ($\rho_H \propto B$, according to Equation 2.3.16) and the longitudinal resistivity remains more or less constant with a slight decrease with the magnetic field. As the magnetic field is increased above 0.4 T up to 1.2 T, the 2DES leaves the classical regime and enters a new regime that is called Shubnikov-de Haas regime. In this regime, the Hall resistivity starts to deviate from the previous linear behavior and the longitudinal resistivity oscillates strongly with magnetic field. These

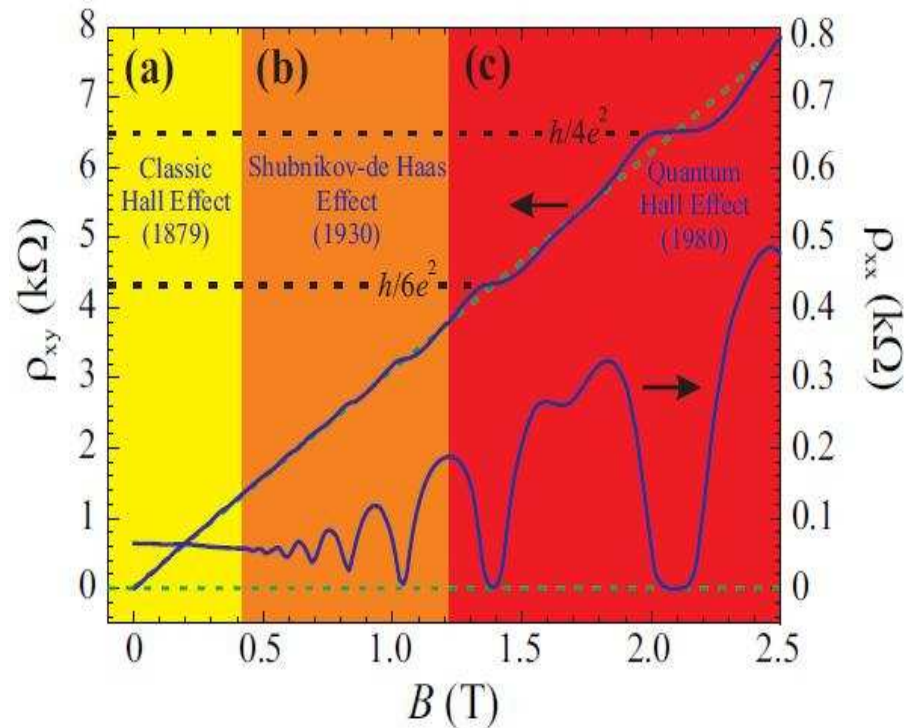


Figure 2.3 A typical magnetotransport curve taken at a QH device with Hall bar geometry. (a) The classical regime: at low magnetic fields the classical Hall effect is observed. (b) Shubnikov-de Haas regime: at high fields the 2DES starts behaving quantum mechanically, such that both Hall resistivity and longitudinal resistivity develop oscillations. (c) The QHE regime: at higher fields longitudinal resistivity goes to zero, and Hall resistivity develops plateaus (Vasile, Ph.D.Thesis, 2007).

oscillations are called Shubnikov-de Haas oscillations which increase with magnetic field. As the magnetic field is further increased, the 2DES enters the quantum Hall effect regime. In this regime, Hall resistivity develops plateaus and the longitudinal resistivity drops to zero.

2.5.1 Integer Quantum Hall Effect (IQHE)

Increasing the magnetic field above 1.2 T, the Hall resistance and longitudinal resistance show the IQHE which was first observed by K. von Klitzing, G. Dorda and

M. Pepper (1980). The IQHE occurs at high magnetic fields and Hall resistance R_H shows some plateaus that are equal to a quantized resistance of $h/(e^2i)$ with an integer $i = \{1, 2, \dots\}$. At the same time the longitudinal resistance goes to zero. One astonishing feature of the IQHE is that a quantized Hall resistance does not depend on the sample geometries and materials. This resistance is only related to two universal constants that are Planck's constant h and elementary charge e . The Hall plateau resistance is measured as $R_{K-90} = 25812.807 \Omega$ and named as the von Klitzing constant. It is accepted as an international resistance standard since 1990. For his discovery, von Klitzing was awarded the Nobel prize for physics in 1985 (Klitzing, 1986).

2.5.2 *Localized and Extended States*

The above discussions of integral quantum Hall effect suggests that the measurements under quantum conditions of temperature and magnetic field the Hall resistance is accurately quantized at 25813.802Ω whether or not the semiconductor is of very high purity and perfection. In real crystals the sharp Landau Levels are broadened due to scattering of electrons (Figure 2.4). These scattering centers (impurities or the positively charged donors) are distributed randomly throughout the 2DES and cause energy fluctuations at the Landau levels. This means that the energy of a Landau level moves up and down throughout the sample (Figure 2.5 (a)). The average magnitude of the fluctuations is equal to the broadening of the Landau levels as shown with the connection lines between in Figure 2.5 (a) and Figure 2.5 (b).

There are two classes of states: delocalized states at the centers of Landau levels, in which the electrons move through the 2DES and localized states, in the tails of the Landau levels, which are captured in the isolated puddles. When the chemical potential μ is in the localized states between the Landau level centers, both the longitudinal resistivity and conductivity become zero $\sigma_{xx} = \rho_{xx} = 0$, and the Hall resistivity ρ_{xy} is quantized. However, when the chemical potential μ is in the extended states, close to

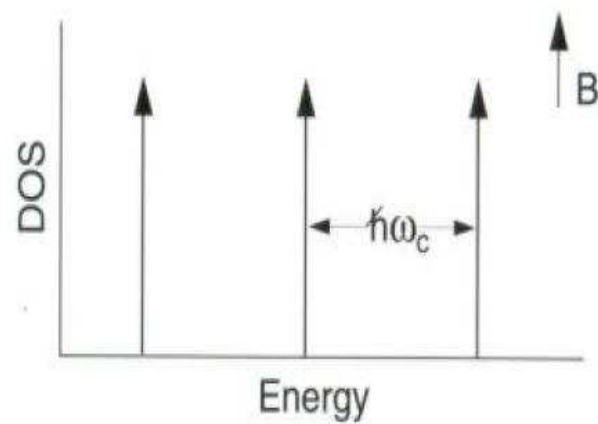


Figure 2.4 Density of states in a 2D electron gas in a strong magnetic field (Ideal crystal) (Stormer, Tsui, & Gossard, 1999).

the Landau level centers, both σ_{xx} and ρ_{xx} are finite, and ρ_{xy} is not quantized.

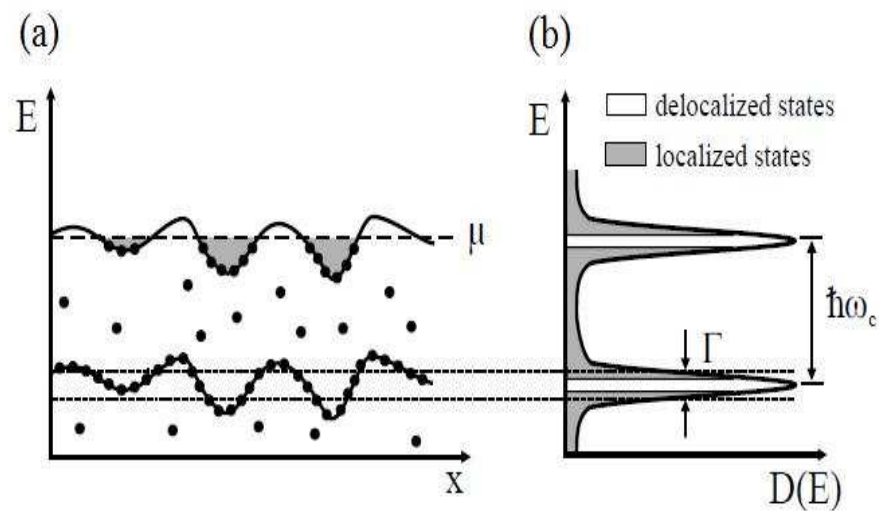


Figure 2.5 Density of states in a 2D electron gas in a strong magnetic field. (Real 2D crystal) (a) Spatial energy fluctuations caused by disorder. (b) Localized and delocalized states (Sagol, Ph.D. Thesis, 2003).

2.5.3 Excitation and Relaxation of Hot Electrons

The Fermi energy is between two adjacent Landau levels (that is band gap) for $T = 0$ K with an integer filling factor ν . The presence of the Fermi level in the band gap leads to a vanishing resistivity $\rho_{xx} = 0$. The resistivity ρ_{xx} is assumed proportional to the number of excited electrons across the band gap.

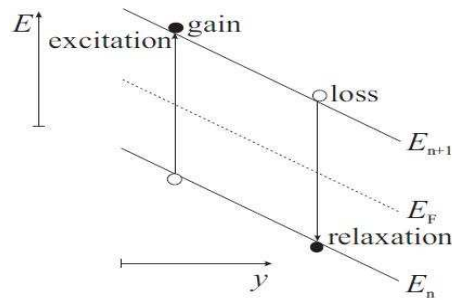


Figure 2.6 The excitation and relaxation between two Landau levels (Vasile, Ph.D.Thesis, 2007).

In Figure 2.6, electrons are excited to the upper LL with a characteristic gain rate due to the Joule heating, and the electrons relax after a certain relaxation time τ_{relax} to the lower LL due to energy loss (electron-phonon scattering). In a real system, the Landau energy levels broaden because of the presence of impurities and disorders (Figure 2.7(a)). The electrons can be excited to upper LLs with the thermal excitation (Figure 2.7(b)). With increasing the temperature of the electron system, their energies increase by the thermal energy $k_B T$ that is comparable with the energy gap between two LLs.

The presence of impurities and disorders induces potential fluctuations (locally enhanced electrical potentials) (Kawaji et al., 1994; Kawaguchi et al., 1995). The potential fluctuations lead to a decrease of the average separation between the LLs. The effects of screening generate quasi-metallic and insulator regions that are called *compressible and incompressible strips* (Figure 2.8). The electron density is constant and

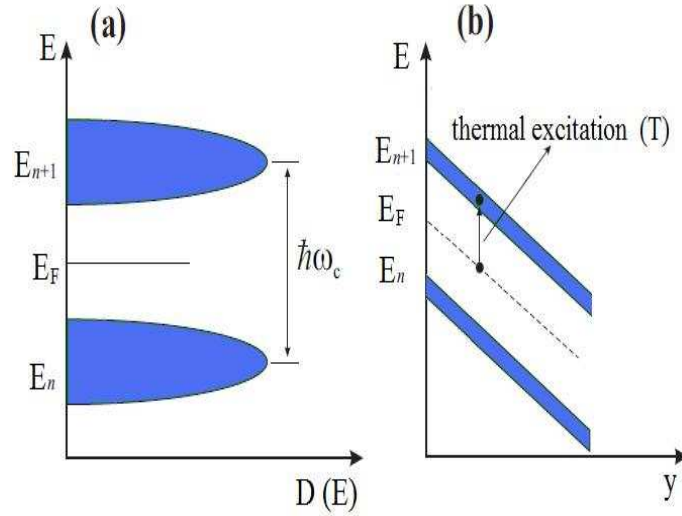


Figure 2.7 (a) Density of states with broad LLs due to the impurities. (b) Thermal excitation in order to excite electrons between 2 LLs.

potential drop occurs. The compressible region do not contribute the flow of current and reduce the effective width of the incompressible regions (strips). The excited electrons to the upper LL come from the IS(s) since the electrons in the compressible regions are localized and do not contribute to the dissipationless current. Since in time, the electrons are excited more and more to the upper LL, the area and the effective width of the IS(s) decreases while the area of compressible regions increases practically linearly with the number of the excited electrons. The shrink of the IS(s) stops when the effective width becomes too small to carry dissipationless current. At this critical moment the density of excited electrons in the upper LL reaches the critical value at which the breakdown of the QHE is complete.

2.5.4 Breakdown of the QHE

Shortly after the discovery of the QHE, the physical limits of the QHE which is called the breakdown phenomenon of the QHE, were investigated in experimentally. The breakdown of the QHE due to high current densities still remains a subject of

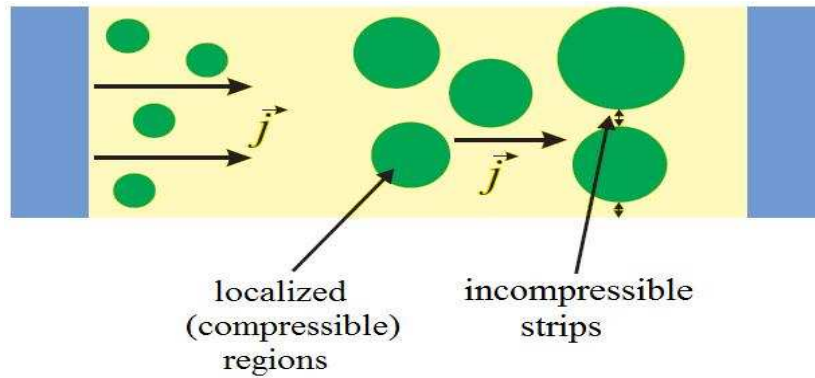


Figure 2.8 Simple sketch of the incompressible strips and compressible regions. In reality this picture would be more complicated since enlarging a compressible region by excitation of electrons from incompressible regions involves always two compressible regions (e.g. a hole-like and an electron-like) with a potential difference equal to the cyclotron energy. Moreover, the compressible regions are induced by local potential landscape and can therefore be of noncircular form (Vasile, Ph.D.Thesis, 2007).

much theoretical and experimental work. On one hand the phenomenon attracts attention because of its importance for the understanding of the QHE. On the other hand, knowledge of the breakdown is crucial for the resistance standard based on the QHE where a critical current as high as possible is aimed at for maximum resolutions (Jeckelmann, & Jeanneret, 2003).

The first experimental study included the current breakdown of the QHE was published by Ebert et al. in 1983. The authors measured the critical current in a series of low mobility GaAs Hall bar devices with different carrier concentrations.

In QHS's, diagonal conductivity σ_{xx} vanishes in the low current regime while the Hall conductivity σ_{xy} is quantized to integer multiples of e^2/h (Klitzing, Dorda, & Pepper, 1980; Akera, 2000; Akera, 2001). With increasing the current up to a critical value, σ_{xx} increases by several orders of magnitude within a narrow range of the current and the QHE breaks down (Ebert, Klitzing, Ploog, & Weimann, 1983; Cage et al., 1983; Kuchar, Bauer, Weimann, & Burkhard, 1984; Akera, 2002.).

Theoretically, otherwise, a hot electron model describes the breakdown of the QHE. It is proposed in this model that the electron heating is responsible for the decrease of σ_{xx} at the breakdown and the electron temperature T_e is the key variable in determining σ_{xx} (Güven et al., 2002; Kaya, Nachtwei, Klitzing, & Eberl, 1998; Ise, Akera, & Suzuura, 2005; Komiyama, Sakuma, Ikushima, & Hirakawa, 2006).

Uchimura and Uemura have applied the hot-electron theory and the self-consistent Born approximation to explain the electric-field dependence of the diagonal conductivity, observed by Kawaji and Wakabayashi, in two-dimensional systems under quantizing magnetic fields (Kawaji, & Wakabayashi, 1976).

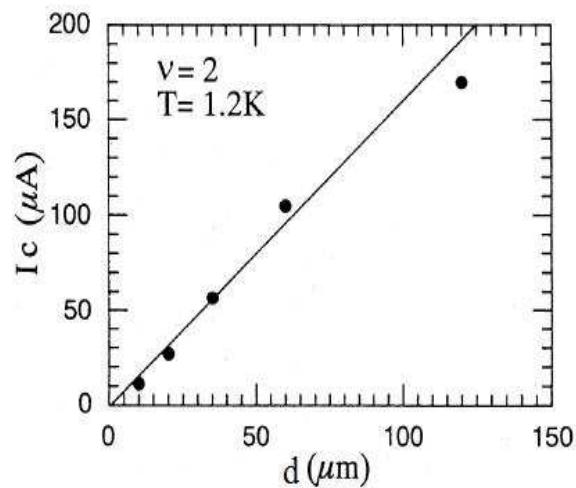


Figure 2.9 Critical current I_c versus device width d for a sample with lower mobilities (Kawaji, Hirakawa, & Nagata, 1993).

Several groups investigate the breakdown current of the QHE as a function of the sample width and obtain two main features. A linear increase of critical current I_c with the sample width was found for samples with low and medium mobilities (typically of the order $10^5 \text{cm}^2/\text{Vs}$) that is shown in Figure 2.9. On the other hand a sublinear dependence for I_c versus sample width was observed for samples of higher mobility (Figure 2.10).

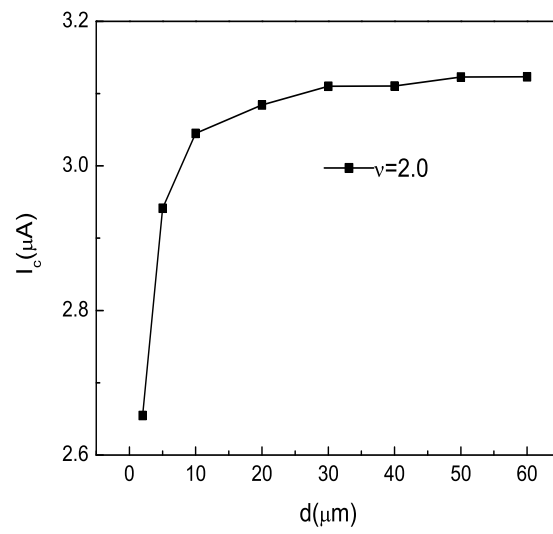


Figure 2.10 Critical current I_c versus device width d for a sample with higher mobilities.

CHAPTER THREE

FUNDAMENTALS OF THE SCREENING THEORY

3.1 Introduction

The spatial distribution of the Hall potential strongly depends on the applied magnetic field B , such that if the system is out of the plateau regime Hall potential varies linearly across the sample resembling the classical Hall effect (Siddiki, & Gerhardt, 2004). In contrast, within the plateaus, the potential presents strong non-linear distributions: At the high B field side of the plateau the potential drop is spread all across the sample indicating that the current is carried at the bulk, meanwhile at the low field side one observes sharp variations at the opposing edges, whereas the potential is constant at the bulk. This behavior is attributed to edge state transport. The spatial variation of the potential drop as a function of B field shows that, while decreasing the field the edge states move towards the physical ends of the sample until the plateau disappears. A simple calculation of the spatial distribution of the edge states, following the original work of Chklovskii et al, shows that the position of the potential drop almost perfectly matches with the position of the edge states. The theoretical work takes into account electron-electron interactions within a Thomas-Fermi approximation (TFA) and provides estimations of the widths and the positions of the compressible and the incompressible strips, for a fixed depletion length. There, it is assumed that the 2DES is separated into compressible (where the Fermi energy is pinned to one of the Landau levels) and incompressible strips (where Fermi energy falls into Landau gap) (Siddiki, & Gerhardt, 2004; Siddiki, Ph.D.Thesis, 2005).

3.2 Thermal Equilibrium

Following Ref.(Chklovskii, Matveev, & Shklovskii, 1993; Oh, & Gerhardt, 1997, Güven, & Gerhardt, 2003) 2DES is modeled as a Hall bar in the $z = 0$ plane, which is subjected to a perpendicular magnetic field $\mathbf{B} = (0, 0, B)$, together with a translational

invariance in x direction.

The electrons are assumed to be confined by the background potential $V_{\text{bg}}(y)$ generated due to ionized donors, which are distributed uniformly in the xy plane. The local electron (number) density is described by $n_{\text{el}}(y)$. To describe the experimental geometries, boundary conditions are imposed such that two metallic gates reside at the physical edges, following Chklovskii et al (Chklovskii, Shklovskii, & Glazman, 1992; Chklovskii, Matveev, & Shklovskii, 1993). The effective potential within the semi-classical approximation can be written as

$$V(y) = V_{\text{bg}}(y) + V_{\text{H}}(y), \quad (3.2.1)$$

with the confinement potential

$$V_{\text{bg}}(y) = -E_{\text{bg}}^0 \sqrt{1 - \left(\frac{y}{d}\right)^2}, \quad E_{\text{bg}}^0 = \frac{2\pi e^2}{\kappa} n_0 d, \quad (3.2.2)$$

and the Hartree potential

$$V_{\text{H}}(y) = \frac{2e^2}{\kappa} \int_{-d}^d dy' K(y, y') n_{\text{el}}(y'). \quad (3.2.3)$$

Here κ is the dielectric constant, n_0 is the donor density and $2d$ is the sample width. Kernel $K(y, y')$ solves the Poisson's equation considering the above mentioned boundary conditions (Siddiki, & Gerhardtts, 2004; Güven, & Gerhardtts, 2003)

$$K(y, y') = \ln \left| \frac{\sqrt{(d^2 - y^2)(d^2 - y'^2)} + d^2 - y'y}{(y - y')d} \right|. \quad (3.2.4)$$

Note the fact that the boundary conditions used in this study result in different Kernel compared to Ref.(Aker, 2001; Kanamaru, Suzuura, & Aker, 2006) and affect the strength of interactions considerably.

The electron density is, in turn, determined by the effective potential $V(y)$ and is calculated within the TFA

$$n_{\text{el}}(y) = \int dE D(E) f(E + V(y) - \mu_{\text{ec}}), \quad (3.2.5)$$

where $D(E)$ is DOS, $f(E)$ is the Fermi function and μ_{ec} is the electrochemical potential that is constant in the equilibrium state (Gerhardts, 2008; Güven, & Gerhardts, 2003; Siddiki, & Gerhardts, 2004).

3.3 Local Equilibrium with Imposed Current

In this work, the local equilibrium approximation, used commonly to describe similar systems is applied (Aker, & Suzuura, 2005). In local equilibrium, the energy distribution of an electron is defined by the Fermi function

$$f(\varepsilon, \mu_{\text{ec}}, T_e) = \frac{1}{\{\exp[(\varepsilon - \mu_{\text{ec}})/k_B T_e] + 1\}}, \quad (3.3.1)$$

where ε is the energy and T_e is the electron temperature. In local equilibrium approximation, the lattice temperature T_L remains unchanged in the presence of an applied current. If an external current is imposed the electrochemical potential $\mu_{\text{ec}}(\mathbf{r})$ depends on position and its gradient $\mathbf{E} = \nabla \mu_{\text{ec}}(\mathbf{r})/e$ satisfies the local Ohm's law

$$\hat{\rho}(\mathbf{r}) \mathbf{j}_{\text{el}}(\mathbf{r}) = \mathbf{E}(\mathbf{r}), \quad (3.3.2)$$

hence local current densities can be obtained if local resistivities are provided. In Eq. 3.3.2, the components of current density $j_{\text{el}y}$ and electric field E_x must be constant due to the translation invariance in the x direction.

$$j_{\text{el}y}(y) \equiv 0, \quad E_x(y) \equiv E_x^0. \quad (3.3.3)$$

The other components are written as

$$j_{n_{\text{el}x}}(y) = \frac{1}{\rho_l(y)} E_x^0, \quad E_y(y) = \frac{\rho_H(y)}{\rho_l(y)} E_x^0, \quad (3.3.4)$$

in terms of the longitudinal component ρ_l and the Hall component ρ_H of the resistivity tensor $\hat{\rho} = \hat{\sigma}^{-1}$. The dissipative current I is the integral of current densities over the sample,

$$I = \int_{-d}^d dy j_{n_{\text{el}x}}(y). \quad (3.3.5)$$

According to the applied current, the constant electric field component along the Hall bar and the Hall voltage across the sample are written as,

$$E_x^0 = I \left[\int_{-d}^d dy \frac{1}{\rho_l(y)} \right]^{-1}, \quad (3.3.6)$$

$$V_H = \int_{-d}^d dy E_y(y) = E_x^0 \int_{-d}^d dy \frac{\rho_H(y)}{\rho_l(y)}, \quad (3.3.7)$$

respectively.

3.4 Result: Lattice Temperature at Position Independent Electron Temperature

Fig. 3.1 and Fig. 3.2 show the filling factor, current density, electrostatic and electrochemical potentials of the Hall bar calculated for different lattice temperatures at fixed magnetic field, $\hbar\omega_c/E_F^0 = 0.909$. Fig. 3.1(a) presents the electron density, with two IS(s) located symmetrically near $x/d = 0.55$ and the surrounding compressible regions. All the electron densities are expressed in terms of local filling given by $\nu(y) = 2\pi n_{\text{el}}(y)l^2$. The width of the IS(s) shrinks with increasing temperature. For $k_B T_L/E_F^0 = 0.02$ and 0.03 clearly visible IS(s) exist. As it seen in Fig.3.1(b) the current density is proportional to the electron density at the highest temperature. With decreasing temperature the 2DES develops IS(s) with low longitudinal resistivity and the current density is increasingly confined to the incompressible regions. Simulta-

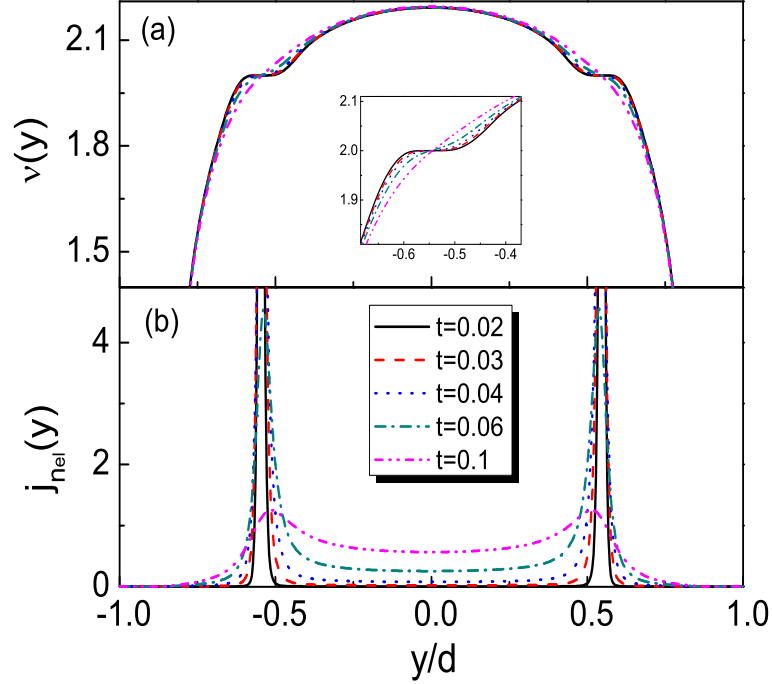


Figure 3.1 (a) Filling factor $\nu(y)$ and (b) current density $j_{nel}(y)$ profiles for the magnetic field $\hbar\omega_c/E_F^0 = 0.909$ at five different temperatures, $t = k_B T_L/E_F^0$. The inset shows the enlarged plateau region.

neously the potentials [Fig.3.2] develop a steplike behavior with variation across the IS(s) and plateaus in the compressible regions.

Fig. 3.3 shows the filling factor profile for varying magnetic field, Ω_c/E_F^0 . For the larger B value, the local filling factor $\nu(y)$ is everywhere in the Hall bar less than 2, and the 2DES is completely compressible. At $\Omega_c/E_F^0 \approx 1$, the center of the sample becomes incompressible and the local filling factor $\nu(y) = 2$. For the lower B value, the filling factor in the center increases and IS(s) with $\nu(y) = 2$ move towards the sample edges and become narrower. At $\Omega_c/E_F^0 \approx 0.5$, IS(s) with local filling factor $\nu(y) = 4$ occur in the center and then move towards the edges. For the lower lattice temperature, this behavior is seen at the lower values of magnetic field.

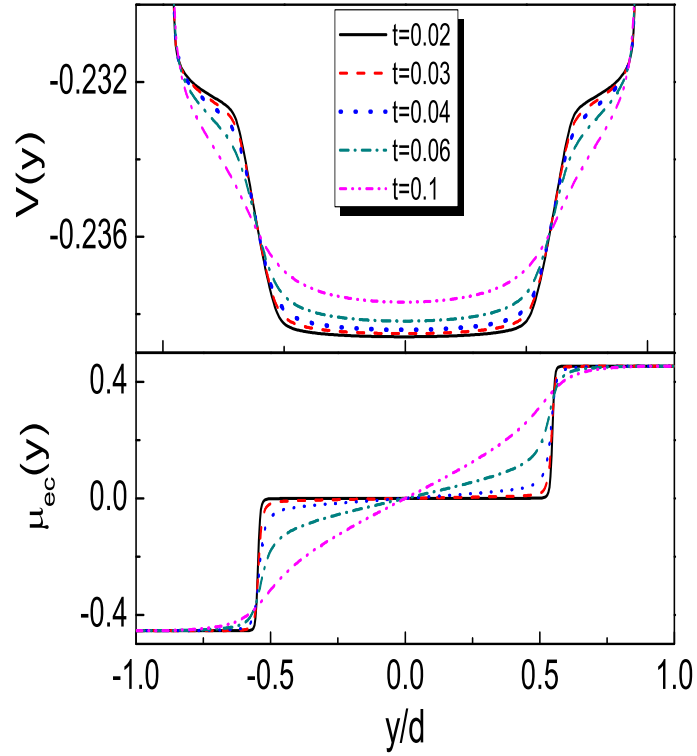


Figure 3.2 Calculated electrostatic $V(y)$ and electrochemical potentials $\mu_{ec}(y)$ for the magnetic field $\hbar\omega_c/E_F^0 = 0.909$ at five temperatures, $k_B T_L/E_F^0$ with Hall bar width $2d = 1\mu\text{m}$.

Fig. 3.4 shows the current distribution for different values of magnetic field, $\Omega_c/E_F^0 = 1.05, 1.0, 0.91$ and 0.83 . For the high magnetic field values $\Omega_c/E_F^0 > 1.0$ there exists no incompressible strip and the current density simply follows the electronic distribution. With decreasing the magnetic field, the current is confined to the intervals where the incompressible strip occurs.

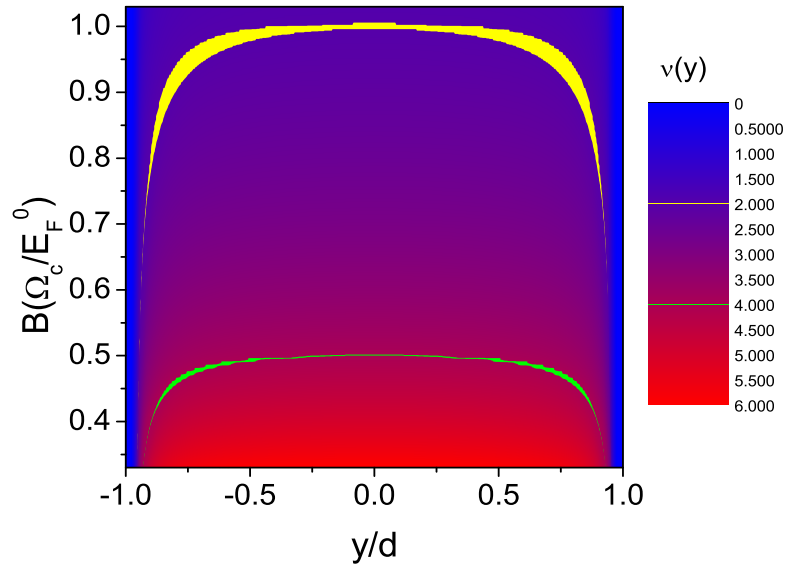


Figure 3.3 Filling factor versus position y and magnetic field ($\Omega_c \equiv \hbar\omega_c$). The regions of incompressible strips with $\nu(y) = 2$ and $\nu(y) = 4$ are indicated.

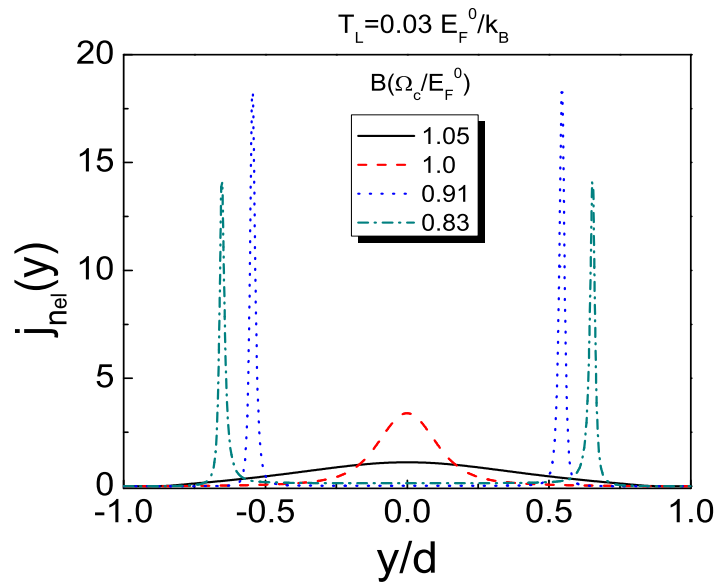


Figure 3.4 Current distribution for different values of magnetic field. Hall bar of width $2d = 1\mu\text{m}$ with the lattice temperature $T_L = 0.03 E_F^0/k_B$.

CHAPTER FOUR

THERMOHYDRODYNAMIC THEORY IN QUANTUM HALL SYSTEMS

4.1 Introduction

Akera and his co-workers developed a theory of thermohydrodynamics in QHS. They described spatial variations of the electron temperature and the chemical potential in the local equilibrium including the nonlinear transport regime with use of the equations of conservation.

4.2 Model, Processes and Macroscopic Variables

4.2.1 Drift and Hopping Processes

Akera and his co-workers consider two types of energy exchange between different locations which are the drift and hopping processes (Akera, 2000; Akera, 2001; Kanamaru, Suzuura, & Akera, 2006). Drift motion perpendicular to the local electric field transfers electrons in extended states between neighboring regions, giving the Hall current perpendicular to the macroscopic electric field (Akera:2001; Akera:2002; Ise, Akera, & Suzuura, 2005; Kanamaru, Suzuura, & Akera, 2006). In the hopping process, a localized wave packet of electron hops in intra-Landau level due to a scattering from other electrons. Therefore, the total number flux density is given by

$$\mathbf{j}_{n_{\text{el}}} = \mathbf{j}_{n_{\text{el}}}^{\text{drift}} + \mathbf{j}_{n_{\text{el}}}^{\text{hop}}. \quad (4.2.1)$$

4.2.2 Model

We consider a 2DES in the plane $z = 0$, with translation invariance in the x direction and an electron density $n_{\text{el}}(y)$ confined to the interval $-d < y < d$. The electrons

are confined in the potential generated due to ionized donors that are distributed uniformly in the $x - y$ plane. We assume local equilibrium, which imposes that the energy distribution of electrons is determined by the Fermi distribution function

$$f(\varepsilon, \mu_{ec}, T_e) = \frac{1}{\{\exp[(\varepsilon - \mu_{ec})/k_B T_e] + 1\}}, \quad (4.2.2)$$

with the electron temperature T_e and the electrochemical (potential) energy μ_{ec} . And also we assume that the phonons are in equilibrium with the lattice temperature T_L and does not change under the applied current.

4.2.3 Macroscopic Variables

Spatial variations of macroscopic variables are taken into account in the thermo-hydrodynamic theory. These variables are the electron temperature $T_e(x, y)$, the electrochemical energy $\mu_{ec}(x, y)$ and the total potential energy $V(x, y)$ which is influenced by the applied current. Instead of solving $V(x, y)$ using electrostatics, $V(x, y)$ is determined by the approximation so that the chemical potential energy is written as $\mu = \mu_{ec} - V$. The variables T_e and μ_{ec} are determined using two hydrodynamic equations given below (Ise, Akera, & Suzuura, 2005).

4.3 Thermo-hydrodynamical Equations

Two hydrodynamic equations are considered and assumed that the electron number and the total energy of the system at hand is conserved. The conservation of the electron number is given by

$$\frac{\partial n_{el}}{\partial t} = -\nabla \cdot \mathbf{j}_{n_{el}}, \quad (4.3.1)$$

where the number flux density is $\mathbf{j}_{n_{el}}$. The energy conservation is formulated by

$$\frac{\partial \varepsilon}{\partial t} = -\nabla \cdot \mathbf{j}_\varepsilon - P_L, \quad (4.3.2)$$

with the energy flux density \mathbf{j}_ε and the energy loss per unit area P_L due to the heat transfer between electrons and phonons (Akera, & Suzuura, 2005). The time evolution of the entropy density s is derived by using Eqs. (4.3.1), (4.3.2), and by the fundamental thermodynamical equation

$$T_e ds = d\varepsilon - \mu_{ec} dn_{el}, \quad (4.3.3)$$

that yields

$$\begin{aligned} T_e \frac{\partial s}{\partial t} &= \frac{\partial \varepsilon}{\partial t} - \mu_{ec} \frac{\partial n_{el}}{\partial t} \\ &= -\nabla \cdot \mathbf{j}_\varepsilon - P_L + \mu_{ec} \nabla \cdot \mathbf{j}_{n_{el}} \\ &= -\nabla \cdot \mathbf{j}_\varepsilon + \mu_{ec} \nabla \cdot \mathbf{j}_{n_{el}} + \nabla \mu_{ec} \cdot \mathbf{j}_{n_{el}} - \nabla \mu_{ec} \cdot \mathbf{j}_{n_{el}} - P_L \\ &= -\nabla \cdot \mathbf{j}_\varepsilon + \nabla (\mu_{ec} \mathbf{j}_{n_{el}}) - \nabla \mu_{ec} \cdot \mathbf{j}_{n_{el}} - P_L \\ &= -\nabla \cdot \underbrace{(\mathbf{j}_\varepsilon - \mu_{ec} \mathbf{j}_{n_{el}})}_{\mathbf{j}_q} - \nabla \mu_{ec} \cdot \mathbf{j}_{n_{el}} - P_L \\ T_e \frac{\partial s}{\partial t} &= -\nabla \cdot \mathbf{j}_q - \nabla \mu_{ec} \cdot \mathbf{j}_{n_{el}} - P_L, \end{aligned} \quad (4.3.4)$$

where the thermal flux density \mathbf{j}_q is described by

$$\mathbf{j}_q = \mathbf{j}_\varepsilon - \mu_{ec} \mathbf{j}_{n_{el}}. \quad (4.3.5)$$

4.3.1 Hopping Components of the Total Flux Densities

4.3.1.1 The Number Flux Density

First we obtain the number flux between neighboring regions due to the hopping process. It is denoted by $J_{n_{el}}^{\text{hop}}$ and is given by

$$J_{n_{el}}^{\text{hop}} = \sum_{\alpha} j_{n_{el}\alpha}^{\text{hop}}, \quad (4.3.6)$$

with the Landau level index α . Each $j_{n_{el}\alpha}^{\text{hop}}$ is induced by the difference of the electron temperature T_e and of in the electrochemical potential μ_{ec} between neighboring regions. In a first order approximation of ΔT_e and $\Delta\mu_{ec}$, $j_{n_{el}\alpha}^{\text{hop}}$ can be written as

$$j_{n_{el}\alpha}^{\text{hop}} = A_{\alpha}\Delta\mu_{ec} + B_{\alpha}\Delta T_e, \quad (4.3.7)$$

with the coefficients A_{α} and B_{α} . These coefficients are related to each other in the hopping process. In the hopping process, the transition rate is ignored when the distance between the wave packets is much large than the magnetic length. Because of this, the wave packets are the corresponding coefficients in the vicinity of the boundary between two regions. The energies of these wave packets are confined within an energy range around $\varepsilon_{\alpha}(x, y) = \varepsilon_{\alpha}^0 + V(x, y)$ with width $\Gamma_{\text{hop}} \sim \Gamma l_{\text{fluc}}$ where Γ is the width of the broadened Landau level and l_{fluc} is the fluctuation length scale. So the occupation probability is given by

$$f_{\alpha} = f(\varepsilon_{\alpha}, \mu_{ec}, T_e) \quad (4.3.8)$$

when $\Gamma_{\text{hop}} \ll k_B T_e$. According to the hopping process between two neighbor regions, $J_{n_{el}\alpha}^{\text{hop}}$ is written as

$$j_{n_{el}\alpha}^{\text{hop}} = -C_{\alpha} [f(\varepsilon_{\alpha}, \mu_{ec} + \Delta\mu_{ec}, T_e + \Delta T_e) - f(\varepsilon_{\alpha}, \mu_{ec}, T_e)]. \quad (4.3.9)$$

The hopping number flux density $j_{n_{el}}^{\text{hop}}$ averaged in the macroscopic scale is written as

$$j_{n_{el}}^{\text{hop}} = - \sum_{\alpha} D_{\alpha} \left(\frac{\partial f_{\alpha}}{\partial \mu_{ec}} \nabla \mu_{ec} + \frac{\partial f_{\alpha}}{\partial T_e} \nabla T_e \right), \quad (4.3.10)$$

with the translation rate of each hopping process D_{α} . Because of the screening, it depends on the disorder potential that is a function of μ and T_e . If the transport coefficients L_{xx}^{11} and L_{xx}^{12} are taken into account, $j_{n_{el}}^{\text{hop}}$ is rewritten as

$$j_{n_{el}}^{\text{hop}} = -L_{xx}^{11} \nabla \mu_{ec} - L_{xx}^{12} T_e^{-1} \nabla T_e. \quad (4.3.11)$$

These coefficients can be solved from Eq. 4.3.10. First L_{xx}^{11} transport coefficient can be solved as following:

$$\frac{\partial f_{\alpha}}{\partial \mu_{ec}} = \frac{\partial}{\partial \mu_{ec}} \left(\frac{1}{\exp[(\varepsilon - \mu_{ec})/k_B T_e] + 1} \right) \quad (4.3.12)$$

$$\left\{ \left(\frac{1}{e^u + 1} \right)' = - \frac{u' e^u}{(e^u + 1)^2} \right\}$$

$$\begin{aligned} \frac{\partial f_{\alpha}}{\partial \mu_{ec}} &= - \left(\frac{-\frac{1}{k_B T_e} \exp[(\varepsilon - \mu_{ec})/k_B T_e]}{(\exp[(\varepsilon - \mu_{ec})/k_B T_e] + 1)^2} \right) \\ &= (k_B T_e)^{-1} \underbrace{\exp[(\varepsilon - \mu_{ec})/k_B T_e]}_{(1-f)/f} \underbrace{\frac{1}{(\exp[(\varepsilon - \mu_{ec})/k_B T_e] + 1)^2}}_{f^2} \\ &= (k_B T_e)^{-1} f_{\alpha} (1 - f_{\alpha}) \end{aligned} \quad (4.3.13)$$

$$L_{xx}^{11} = \frac{\sigma_{xx}}{e^2} = (k_B T_e)^{-1} \sum_{\alpha} D_{\alpha} f_{\alpha} (1 - f_{\alpha}). \quad (4.3.14)$$

Next the L_{xx}^{12} transport coefficient can be solved, and obtained as

$$\frac{\partial f_{\alpha}}{\partial T_e} = \frac{\partial}{\partial T_e} \left(\frac{1}{\exp[(\varepsilon - \mu_{ec})/k_B T_e] + 1} \right) \quad (4.3.15)$$

$$\begin{aligned}
\frac{\partial f_\alpha}{\partial T_e} &= \frac{\partial}{\partial T_e} \left(\exp \left[\left(\frac{\varepsilon - \mu_{ec}}{k_B} \right) T_e^{-1} \right] + 1 \right)^{-1} \\
&= \underbrace{\left(\exp \left[\left(\frac{\varepsilon - \mu_{ec}}{k_B} \right) T_e^{-1} \right] + 1 \right)^{-2}}_{f^2} \left(\left(\frac{\varepsilon - \mu_{ec}}{k_B T_e} \right) T_e^{-1} \right) \underbrace{\exp \left[\left(\frac{\varepsilon - \mu_{ec}}{k_B} \right) T_e^{-1} \right]}_{(1-f)/f} \\
&= (\varepsilon - \mu_{ec})(k_B T_e)^{-1} T_e^{-1} f_\alpha (1 - f_\alpha)
\end{aligned} \tag{4.3.16}$$

$$L_{xx}^{12} = (k_B T_e)^{-1} \sum_{\alpha} D_{\alpha} f_{\alpha} (1 - f_{\alpha}) (\varepsilon_{\alpha}^0 - \mu). \tag{4.3.17}$$

Therefore, the number flux density depending on hopping component j_{nel}^{hop} is obtained including the transport coefficients L_{xx}^{11} and L_{xx}^{12}

$$j_{nel}^{\text{hop}} = -L_{xx}^{11} \nabla \mu_{ec} - L_{xx}^{12} T_e^{-1} \nabla T_e. \tag{4.3.18}$$

The L_{xx}^{11} and L_{xx}^{12} coefficients are functions of T_e and μ . In the linear response regime, these coefficients are to be evaluated in equilibrium.

4.3.1.2 The Thermal Flux Density

The thermal flux density is given by

$$\begin{aligned}
\mathbf{j}_q &= \mathbf{j}_{\varepsilon} - \mu_{ec} \mathbf{j}_{nel} \\
&= (\varepsilon_{\alpha} - \mu_{ec}) \mathbf{j}_{nel}.
\end{aligned} \tag{4.3.19}$$

In hopping process, this equation is written as

$$j_q^{\text{hop}} = - \sum_{\alpha} (\varepsilon_{\alpha} - \mu_{ec}) D_{\alpha} \left(\frac{\partial f_{\alpha}}{\partial \mu_{ec}} \nabla \mu_{ec} + \frac{\partial f_{\alpha}}{\partial T_e} \nabla T_e \right). \tag{4.3.20}$$

This equation means that an electron in the Landau level carries a thermal energy ($\epsilon_\alpha - \mu_{ec}$). This equation is rewritten as

$$j_q^{\text{hop}} = -L_{xx}^{21} \nabla \mu_{ec} - L_{xx}^{22} T_e^{-1} \nabla T_e, \quad (4.3.21)$$

related to the L_{xx}^{21} and L_{xx}^{22} transport coefficients. In order to solve L_{xx}^{21} transport coefficient, the following expression

$$\frac{\partial f_\alpha}{\partial \mu_{ec}} = (k_B T_e)^{-1} f_\alpha (1 - f_\alpha) \quad (4.3.22)$$

is substituted in Eq. 4.3.20. Then L_{xx}^{21} transport coefficient is obtained as

$$L_{xx}^{21} = (k_B T_e)^{-1} \sum_{\alpha} D_{\alpha} f_{\alpha} (1 - f_{\alpha}) (\epsilon_{\alpha}^0 - \mu_{ec}) \quad (4.3.23)$$

and this expression shows that $L_{xx}^{21} = L_{xx}^{12}$.

L_{xx}^{22} transport coefficient is calculated by using

$$\frac{\partial f_{\alpha}}{\partial T_e} = (\epsilon_{\alpha}^0 - \mu_{ec}) (k_B T_e)^{-1} T_e^{-1} f_{\alpha} (1 - f_{\alpha}). \quad (4.3.24)$$

Substituting this expression in Eq. 4.3.20, L_{xx}^{22} transport coefficient is given by

$$L_{xx}^{22} = (k_B T_e)^{-1} \sum_{\alpha} D_{\alpha} f_{\alpha} (1 - f_{\alpha}) (\epsilon_{\alpha}^0 - \mu)^2. \quad (4.3.25)$$

4.3.2 Drift Components of the Total Flux Densities

The local potential V_{loc} contains the random potential, so that the local flux density fluctuates spatially due to the drift motion. The macroscopic flux density is determined by using the average of the local flux density. In order to obtain the macroscopic number flux density $j_{n_{e|\alpha}}^{\text{drift}}$ in the Landau level α , the drift velocity \mathbf{v} should be rewritten

as

$$\mathbf{v} = \frac{\mathbf{E} \times \mathbf{B}}{B^2}.$$

$$\mathbf{E} \times \mathbf{B} = \begin{pmatrix} \hat{i} & \hat{j} & \hat{k} \\ E_x & E_y & E_z \\ 0 & 0 & B_z \end{pmatrix} = \hat{i}(E_y B_z) - \hat{j}(E_x B_z)$$

$$E_x = \frac{1}{e} \nabla_x V_{\text{loc}}, \quad E_y = \frac{1}{e} \nabla_y V_{\text{loc}}$$

$$\mathbf{E} \times \mathbf{B} = \frac{1}{e} \begin{pmatrix} 0 & 1 \\ -1 & 0 \end{pmatrix} \begin{pmatrix} \nabla_x V_{\text{loc}} \\ \nabla_y V_{\text{loc}} \end{pmatrix} \mathbf{B}$$

$$\hat{\varepsilon} = \begin{pmatrix} 0 & 1 \\ -1 & 0 \end{pmatrix}, \quad s_B = \frac{B}{|B|} \text{ and } l^2 = \hbar/(eB)$$

$$\mathbf{v} = \frac{1}{eB} \frac{\mathbf{B}}{B} \hat{\varepsilon} \nabla V_{\text{loc}} \quad (4.3.26)$$

$$= \frac{l^2}{\hbar} s_B \hat{\varepsilon} \nabla V_{\text{loc}}. \quad (4.3.27)$$

After substituting the drift velocity \mathbf{v} in $\mathbf{j} = -n_{\text{el}} e \mathbf{v}$, $j_{n_{\text{el}}\alpha}^{\text{drift}}$ is obtained as

$$j_{n_{\text{el}}\alpha}^{\text{drift}} = \langle f(\varepsilon_{\alpha}^0 + V_{\text{loc}}, \mu_{\text{ec}}, T_e) h^{-1} s_B \hat{\varepsilon} \nabla V_{\text{loc}} \rangle_{\text{av}}. \quad (4.3.28)$$

The occupation probability of localized states can be replaced by that of extended states, since localized states have no contributions to the macroscopic flux density. Therefore, the number flux density in the Landau level $j_{n_{\text{el}}\alpha}^{\text{drift}}$ is given by

$$j_{n_{\text{el}}\alpha}^{\text{drift}} = f(\varepsilon_{\alpha}^0 + V, \mu_{\text{ec}}, T_e) \langle h^{-1} s_B \hat{\varepsilon} \nabla V_{\text{loc}} \rangle_{\text{av}}. \quad (4.3.29)$$

Since the spatial average of ∇V_{loc} is equal to ∇V , the number flux density $j_{n_{\text{el}}}^{\text{drift}}$ which is the sum of the Landau levels, is given by

$$j_{n_{\text{el}}}^{\text{drift}} = L_{yx}^{11} \hat{\epsilon} \nabla V. \quad (4.3.30)$$

It is clearly seen that L_{yx}^{11} transport coefficient is

$$L_{yx}^{11} = \frac{\sigma_{yx}}{e^2} = \frac{s_B}{h} \sum_{\alpha} f_{\alpha}. \quad (4.3.31)$$

The thermal flux density

$$j_{q\alpha}^{\text{drift}} = (\epsilon_{\alpha}^0 - \mu) f(\epsilon_{\alpha}^0 + V, \mu_{\text{ec}}, T_e) < h^{-1} s_B \hat{\epsilon} \nabla V_{\text{loc}} >_{\text{av}} \quad (4.3.32)$$

includes K_{yx}^{21} transport coefficient which is given by

$$K_{yx}^{21} = \frac{s_B}{h} \sum_{\alpha} (\epsilon_{\alpha}^0 - \mu) f_{\alpha}. \quad (4.3.33)$$

Accordingly the transport coefficients L_{yx}^{11} and K_{yx}^{21} are rewritten as

$$L_{yx}^{11} = s_B \frac{2\pi l^2}{h} n_0, \quad (4.3.34)$$

$$K_{yx}^{21} = s_B \frac{2\pi l^2}{h} (T_e s_0), \quad (4.3.35)$$

with the thermohydrodynamic quantities n_0 , Ω_0 and s_0 . Here Ω_0 is the thermodynamic potential density given by

$$\Omega_0(T_e, \mu, B) = -\frac{k_B T_e}{2\pi l^2} \sum_{\alpha} \ln \left[1 + \exp \left(-\frac{\epsilon_{\alpha}^0 - \mu}{k_B T_e} \right) \right]. \quad (4.3.36)$$

The electron density n_0 is defined as

$$n_0 = - \left(\frac{\partial \Omega_0}{\partial \mu} \right)_{T_e, B}, \quad (4.3.37)$$

and the entropy density s_0 is determined as

$$s_0 = - \left(\frac{\partial \Omega_0}{\partial T_e} \right)_{\mu, B}. \quad (4.3.38)$$

The electron density n_0 is obtained as following:

$$\begin{aligned} n_0 &= - \left(\frac{\partial \Omega_0}{\partial \mu} \right)_{T_e, B} \\ &= - \frac{\partial}{\partial \mu} \left(- \frac{k_B T_e}{2\pi l^2} \sum_{\alpha} \ln \left[1 + \exp \left(- \frac{\varepsilon_{\alpha}^0 - \mu}{k_B T_e} \right) \right] \right) \\ &= \frac{k_B T_e}{2\pi l^2} \sum_{\alpha} \frac{\partial}{\partial \mu} \left(\ln \left[1 + \exp \left(- \frac{\varepsilon_{\alpha}^0 - \mu}{k_B T_e} \right) \right] \right) \\ &= \frac{k_B T_e}{2\pi l^2} \sum_{\alpha} \frac{\frac{\partial}{\partial \mu} \left(1 + \exp \left(- \frac{\varepsilon_{\alpha}^0 - \mu}{k_B T_e} \right) \right)}{\left(1 + \exp \left(- \frac{\varepsilon_{\alpha}^0 - \mu}{k_B T_e} \right) \right)} \\ &= \frac{k_B T_e}{2\pi l^2} \sum_{\alpha} \frac{(k_B T_e)^{-1} \exp \left(- \frac{\varepsilon_{\alpha}^0 - \mu}{k_B T_e} \right)}{\left(1 + \exp \left(- \frac{\varepsilon_{\alpha}^0 - \mu}{k_B T_e} \right) \right)} \\ &= \frac{k_B T_e}{2\pi l^2} \sum_{\alpha} (k_B T_e)^{-1} \left(\frac{f_{\alpha}}{1 - f_{\alpha}} \right) (1 - f_{\alpha}) \\ n_0 &= \frac{1}{2\pi l^2} \sum_{\alpha} f_{\alpha}. \end{aligned} \quad (4.3.40)$$

By substituting this into Eq.4.3.34, the transport coefficient L_{yx}^{11} is rewritten as

$$\begin{aligned} L_{yx}^{11} &= s_B \frac{2\pi l^2}{h} \frac{1}{2\pi l^2} \sum_{\alpha} f_{\alpha}, \\ L_{yx}^{11} &= \frac{s_B}{h} \sum_{\alpha} f_{\alpha}. \end{aligned} \quad (4.3.41)$$

Similarly, the entropy density s_0 can be expressed as

$$\begin{aligned}
s_0 &= - \left(\frac{\partial \Omega_0}{\partial T_e} \right)_{\mu, B} \\
&= - \frac{\partial}{\partial T_e} \left(- \frac{k_B T_e}{2\pi l^2} \sum_{\alpha} \ln \left[1 + \exp \left(- \frac{\epsilon_{\alpha}^0 - \mu}{k_B T_e} \right) \right] \right) \\
&= \frac{k_B T_e}{2\pi l^2} \sum_{\alpha} \frac{\partial}{\partial T_e} \left(\ln \left[1 + \exp \left(- \frac{\epsilon_{\alpha}^0 - \mu}{k_B T_e} \right) \right] \right) \\
&= \frac{k_B T_e}{2\pi l^2} \sum_{\alpha} \frac{\frac{\partial}{\partial T_e} \left(1 + \exp \left(- \frac{\epsilon_{\alpha}^0 - \mu}{k_B T_e} \right) \right)}{\left(1 + \exp \left(- \frac{\epsilon_{\alpha}^0 - \mu}{k_B T_e} \right) \right)} \\
&= \frac{k_B T_e}{2\pi l^2} \sum_{\alpha} \frac{(\epsilon_{\alpha}^0 - \mu)(k_B T_e)^{-1} T_e^{-1} \exp \left(- \frac{\epsilon_{\alpha}^0 - \mu}{k_B T_e} \right)}{\left(1 + \exp \left(- \frac{\epsilon_{\alpha}^0 - \mu}{k_B T_e} \right) \right)} \\
&= \frac{k_B T_e}{2\pi l^2} \sum_{\alpha} \left((\epsilon_{\alpha}^0 - \mu)(k_B T_e)^{-1} T_e^{-1} \right) \left(\frac{f_{\alpha}}{1 - f_{\alpha}} \right) (1 - f_{\alpha}) \\
s_0 &= \frac{T_e^{-1}}{2\pi l^2} \sum_{\alpha} (\epsilon_{\alpha}^0 - \mu) f_{\alpha}.
\end{aligned} \tag{4.3.42}$$

Additionally by substituting this into Eq.4.3.35, the transport coefficient K_{yx}^{21} is found as

$$\begin{aligned}
K_{yx}^{21} &= s_B \frac{2\pi l^2}{h} (\Omega_0 + T_e s_0) \\
&= s_B \frac{2\pi l^2}{h} T_e \left(- \frac{k_B T_e}{2\pi l^2} \sum_{\alpha} \ln \left[1 + \exp \left(- \frac{\epsilon_{\alpha}^0 - \mu}{k_B T_e} \right) \right] \right) + \\
&\quad T_e \sum_{\alpha} \frac{k_B}{2\pi l^2} \ln \left[1 + \exp \left(- \frac{\epsilon_{\alpha}^0 - \mu}{k_B T_e} \right) \right] + \\
&\quad \sum_{\alpha} \frac{k_B T_e}{2\pi l^2} (k_B T_e)^{-1} (\epsilon_{\alpha}^0 - \mu) f_{\alpha} \\
&= \frac{s_B}{h} \sum_{\alpha} (\epsilon_{\alpha}^0 - \mu) f_{\alpha}.
\end{aligned} \tag{4.3.44}$$

4.3.3 Total Flux Densities

The number flux density $\mathbf{j}_{n_{el}}$ is caused by the transitions of the electrons. On the other hand the thermal flux density is generated by the motion of the electrons. The total flux density is defined by

$$\begin{aligned}\mathbf{j}_{n_{el}} &= \mathbf{j}_{n_{el}}^{\text{hop}} + \mathbf{j}_{n_{el}}^{\text{drift}}, \\ \mathbf{j}_q &= \mathbf{j}_q^{\text{hop}} + \mathbf{j}_q^{\text{drift}}.\end{aligned}\quad (4.3.45)$$

in terms of the drift and hopping components. Utilizing the above equations that describe the drift and hopping processes, the total flux densities can be summarized as (Akera, & Suzuura, 2005)

$$j_{n_{el}}(x) = -L_{xx}^{11} \nabla_x \mu_{ec} + L_{yx}^{11} \nabla_y V - L_{xx}^{12} T_e^{-1} \nabla_x T_e, \quad (4.3.46)$$

$$j_{n_{el}}(y) = -L_{yx}^{11} \nabla_x V - L_{xx}^{11} \nabla_y \mu_{ec} - L_{xx}^{12} T_e^{-1} \nabla_y T_e, \quad (4.3.47)$$

$$j_q(x) = -L_{xx}^{12} \nabla_x \mu_{ec} + K_{yx}^{21} \nabla_y V - L_{xx}^{22} T_e^{-1} \nabla_x T_e, \quad (4.3.48)$$

$$j_q(y) = -K_{yx}^{21} \nabla_x V - L_{xx}^{12} \nabla_y \mu_{ec} - L_{xx}^{22} T_e^{-1} \nabla_y T_e. \quad (4.3.49)$$

4.3.4 Transport Coefficients

The transport coefficients are defined as

$$L_{xx}^{11} = e^{-2} \sigma_{xx} = 2(k_B T_e)^{-1} \sum_{\alpha} D_{\alpha} f_{\alpha} (1 - f_{\alpha}), \quad (4.3.50)$$

$$L_{xx}^{12} = L_{xx}^{21} = 2(k_B T_e)^{-1} \sum_{\alpha} D_{\alpha} (\varepsilon_{\alpha} - \mu) f_{\alpha} (1 - f_{\alpha}), \quad (4.3.51)$$

$$L_{xx}^{22} = 2(k_B T_e)^{-1} \sum_{\alpha} D_{\alpha} (\varepsilon_{\alpha} - \mu)^2 f_{\alpha} (1 - f_{\alpha}), \quad (4.3.52)$$

$$L_{yx}^{11} = e^{-2} \sigma_{yx} = \frac{2}{h} \sum_{\alpha} f_{\alpha}, \quad (4.3.53)$$

$$K_{yx}^{21} = \frac{2}{h} \sum_{\alpha} (\varepsilon_{\alpha} - \mu) f_{\alpha}. \quad (4.3.54)$$

with the energy of the α -th Landau level without the potential $\varepsilon_{\alpha} = \hbar \omega_c (\alpha + 1/2)$ and the chemical potential $\mu = \mu_{ec} - V$. The occupation probability f_{α} is defined by

$$f_{\alpha} = f(\varepsilon_{\alpha}, \mu, T_e), \quad (4.3.55)$$

with the electron temperature T_e . The coefficient D_{α} is due to hopping process and is written as

$$D_{\alpha} = (2\alpha + 1)D_0, \quad (4.3.56)$$

with D_0 coefficient for $\alpha = 0$. The parameter D_0 gives the saturation value of the conductivity σ_{xx} in the high temperature limit ($k_B T_e \gg \hbar \omega_c$). D_0 is taken $23.3 \times 10^{-3} E_0 / \hbar$ from the experimental results by Komiyama et al (Kanamaru, Suzuura, & Akera, 2006).

4.3.5 Boundary Conditions and Edge Current

The translation invariance in the x direction is assumed in this study. Therefore the electron temperature T_e and the chemical potential μ are independent of x direction.

Also electric field E_x in x direction becomes $E_x = \nabla_x(\Delta V)/e$ because of $\nabla_x(\Delta\mu) = 0$. The boundary conditions must be applied to the equations of conservation. In this system, the electrons are confined by the potential produced by the donors. This potential is infinite outside the sample, $V(y) = \infty$ for $|y| > d$. Therefore, the flux is absent in this region. Then, the boundary conditions at $-d < y < d$ are defined by

$$j_{n_{el}y} = 0, \quad (4.3.57)$$

$$j_{qy} = -eE_x J_{n_{el}}^{\text{edge}}, \quad (4.3.58)$$

with the number flux $J_{n_{el}}^{\text{edge}}$ along the edge of the sample . (Kanamaru, Suzuura, & Akera, 2006).

The fluxes at the edge regions are called drift fluxes. The coordinates (ξ, η) are introduced for each boundary of the 2DES. The unit vector is labeled by \mathbf{n} . The η and the ξ axes along the boundary are taken in the direction of \mathbf{n} and $\hat{\mathbf{n}}$, respectively. The fluxes are calculated in the edge region $\eta_{\text{edge}} < \eta < \eta_{\text{edge}} + \Delta\eta$. The electron and the flux densities can be ignored in the region $\eta > \eta_{\text{edge}} + \Delta\eta$. The hopping flux is ignored in the edge region, since $\Delta\eta$ is small in the present steep confining potential. So that the drift flux is taken into account. The gradient of the confining potential is large (Akera, & Suzuura, 2005). The drift number flux is defined by

$$\mathbf{J}_{n_{el}}^{\text{edge}} = \int_{\eta_{\text{edge}}}^{\eta_{\text{edge}} + \Delta\eta} \mathbf{j}_{n_{el}}^{\text{drift}} d\eta. \quad (4.3.59)$$

$\mathbf{j}_{n_{el}}^{\text{drift}}$ and L_{yx}^{11} are given by

$$\mathbf{j}_{n_{el}}^{\text{drift}} = L_{yx}^{11} \hat{\mathbf{n}} \nabla V, \quad L_{yx}^{11} = \frac{s_B}{h} \sum_{\alpha} f_{\alpha},$$

respectively. Using these equations, \mathbf{J}_{nel}^{edge} should be rewritten as

$$\mathbf{J}_{nel}^{edge} = \underbrace{\frac{s_B}{h} \sum_{\alpha} \int_{\eta_{edge}}^{\eta_{edge} + \Delta\eta} d\eta \frac{\partial V}{\partial \eta} f(\epsilon_{\alpha}^0 + V, \mu_{ec}, T_e)}_{K_{nel}} \hat{\mathbf{n}} \quad (4.3.60)$$

$$K_{nel} = \frac{s_B}{h} \sum_{\alpha} \int_{\eta_{edge}}^{\eta_{edge} + \Delta\eta} d\eta \frac{\partial V}{\partial \eta} f(\epsilon_{\alpha}^0 + V, \mu_{ec}, T_e) \quad (4.3.61)$$

$$\mathbf{J}_{nel}^{edge} = K_{nel} \hat{\mathbf{n}}. \quad (4.3.62)$$

η dependence of μ_{ec} and T_e can be ignored, so that only energy dependence is taken into account.

$$\begin{aligned} K_{nel} &= \frac{s_B}{h} \sum_{\alpha} \int_{\epsilon_{\alpha}}^{\infty} f(\epsilon, \mu_{ec}, T_e) d\epsilon \\ &= \frac{s_B}{h} \sum_{\alpha} \int_{\epsilon_{\alpha}}^{\infty} \frac{1}{\exp\left(\frac{\epsilon - \mu_{ec}}{k_B T_e}\right) + 1} d\epsilon \end{aligned} \quad (4.3.63)$$

$$\begin{aligned} K_{nel} &= -\frac{s_B}{h} k_B T_e \sum_{\alpha} \left[\ln \left(1 + \exp \left(-\frac{\epsilon_{\alpha} - \mu_{ec}}{k_B T_e} \right) \right) \right] \\ &= \frac{s_B}{h} k_B T_e \sum_{\alpha} \left[\ln \left(1 + \exp \left(-\frac{\epsilon_{\alpha}^0 - \mu}{k_B T_e} \right) \right) \right] \end{aligned} \quad (4.3.64)$$

Using Eq. 4.3.36 K_{nel} should be rewritten as

$$K_{nel} = -\frac{s_B}{h} 2\pi l^2 \Omega_0, \quad (4.3.65)$$

with the thermodynamic potential density Ω_0 . According to this equation, $\partial K_{nel} / \partial \mu$ is obtained as

$$\frac{\partial K_{nel}}{\partial \mu} = -s_B \frac{2\pi l^2}{h} \frac{\partial \Omega_0}{\partial \mu}. \quad (4.3.66)$$

Using the following equation

$$\left(\frac{\partial\Omega_0}{\partial\mu}\right)_{T_e,B} = -n_0 = -\frac{1}{2\pi l^2} \sum_{\alpha} f_{\alpha},$$

$\partial K_{nel}/\partial\mu$ should be rewritten as

$$\begin{aligned} \frac{\partial K_{nel}}{\partial\mu} &= \frac{s_B}{h} \sum_{\alpha} f_{\alpha}, \\ &= L_{yx}^{11}. \end{aligned} \quad (4.3.67)$$

Similarly, $\partial K_{nel}/\partial T_e$ can be written as

$$\frac{\partial K_{nel}}{\partial T_e} = -s_B \frac{2\pi l^2}{h} \frac{\partial\Omega_0}{\partial T_e}. \quad (4.3.68)$$

$$\left(\frac{\partial\Omega_0}{\partial\mu}\right)_{T_e,B} = -s_0 = -\frac{T_e^{-1}}{2\pi l^2} \sum_{\alpha} (\epsilon_{\alpha}^0 - \mu) f_{\alpha}$$

Substituting this expression in Eq. 4.3.68, $\partial K_{nel}/\partial T_e$ is found as

$$\begin{aligned} \frac{\partial K_{nel}}{\partial T_e} &= \frac{1}{T_e} \frac{s_B}{h} \sum_{\alpha} (\epsilon_{\alpha}^0 - \mu) f_{\alpha}, \\ &= \frac{1}{T_e} L_{yx}^{12}. \end{aligned} \quad (4.3.69)$$

Finally,

$$L_{yx}^{12} = K_{yx}^{21} + K_n.$$

4.3.6 Energy Loss

The boundary conditions presented in the previous section, are used in the equations of conservation, Eq.4.3.1 and 4.3.2;

$$\Delta j_{nel y} = 0 \quad (-d < y < d), \quad (4.3.70)$$

$$\nabla_y(\Delta j_{qy}) + eE_x j_{n_{el}x} + P_L = 0. \quad (4.3.71)$$

with the deviations from the equilibrium values. Here P_L is the energy loss due to the heat transfer between electron and lattice. It is a function of μ , T_e and T_L and defined by (Akera, & Suzuura, 2005).

$$P_L = C_p(T_e - T_L), \quad (4.3.72)$$

with

$$C_p = C_p^0 \int d\varepsilon \rho(\varepsilon) \left(-\frac{\partial f(\varepsilon + V, \mu_{ec}, T_e)}{\partial \varepsilon} \right). \quad (4.3.73)$$

C_p includes the density of state $\rho(\varepsilon)$ written as

$$\rho(\varepsilon) = \frac{1}{\pi l^2} \sum_{\alpha} \frac{1}{\sqrt{\pi} \Gamma_L} \exp \left[-\frac{(\varepsilon_{\alpha} - \varepsilon)^2}{\Gamma_L^2} \right], \quad (4.3.74)$$

where Γ_L is the Landau level broadening (Kanamaru, Suzuura, & Akera, 2006). The coefficient C_p^0 is defined by the transition rate due to electron-phonon scattering and is estimated to be $1.4 \times 10^{-5} k_B E_0^2 / \hbar$ from the experimental results by Komiyama *et al* (Komiyama, Takamasu, Hiyamizu, & Sasa, 1985).

CHAPTER FIVE

POSITION DEPENDENT ELECTRON TEMPERATURE - RESULTS

5.1 Introduction

The spatial distribution of the current density and the electrochemical potential under quantizing magnetic fields at low temperatures in 2DES, are extensively investigated in recent years (Ise, Akera, & Suzuura, 2005; Komiyama, Sakuma, Ikushima, & Hirakawa, 2006; Akera, & Suzuura, 2005). Güven and Gerhardtts calculated the spatial distribution of the current density $\mathbf{j}_{nel}(x, y)$ and position-dependent electrochemical potential $\mu_{ec}(x, y)$ utilizing a local version of the Ohm's law, starting from the electrostatic quantities obtained within a self-consistent Thomas-Fermi-Poisson approximation (TFPA) to include classical electron-electron (Hartree) interaction (Siddiki, & Gerhardtts, 2003; Siddiki, 2007; Siddiki, & Marquardt, 2007). This approach is known as the screening theory of the integer quantized Hall effect and it was briefly discussed in Chapter 3. In screening theory, heating effects were neglected hence the electron temperature T_e is assumed to be uniform through the system and equals to the lattice temperature T_L (Gerhardtts, 2008). Subsequently Akera and his co-workers implemented the above mentioned calculation scheme, however, also by solving the thermohydrodynamical equations they were able to describe dissipative effects and thereby obtain the spatial distribution of the electron temperature (Kanamaru, Suzuura, & Akera, 2006). They showed that, the current carrying IS(s) strongly affect the electron temperature. The electrostatic boundary conditions imposed in this work are viable mainly for a homogeneous system, however, becomes questionable when considering realistic samples. In any case, this approach opens a new window to investigate the heating effects at a microscopic level and provides reasonable estimates when compared to experiments.

In this chapter, the spatial dependence of electron temperature is represented in QHS, where compressible and incompressible strips are present as a result of interactions. To investigate the spatial distribution of the local electron temperature, the

theory of thermo-hydrodynamics which is bound by conservation of electron number and thermal flux densities is employed following Akera and his co-workers (Akera, 2000; Akera, 2001; Kanamaru, Suzuura, & Akera, 2006). This investigation differs from these pioneering works, since the realistic boundary conditions are imposed and therefore describe experimental systems accurately. This enables us to predict an unexpected behavior that can be observed in the QHS based Aharonov-Bohm interference experiments, which is dictated by the local electron temperature variations.

5.2 Electron Temperature and Current Density

5.2.1 Lattice Temperature Dependence

While presenting the results, Fermi energy at the center E_F^0 of the 2DES is considered as the energy scale, since this quantity remains constant once the sample properties (e.g. depletion length, n_0 etc.) are fixed, whereas the cyclotron frequency $\omega_c = eB/(mc)$ is used to denote the field strength. The magnetic length $\ell = \sqrt{eB/\hbar}$ provides a length scale, quantifying the importance of quantum mechanical effects such as the width of the wave function. As commonly used, the filling factor $\nu = 2\pi\ell^2 n_{el}$ describes the occupation of the Landau levels. If electron density exactly equals to the magnetic flux (number) density, the Landau level is fully occupied and ν is an integer. This situation is called an incompressible state, where no states are available at the Fermi energy. Hence, within an incompressible state, electron density distribution is constant. It is straightforward to define the local version of the filling factor by $\nu(x,y) = 2\pi\ell^2 n_{el}(x,y)$.

First the effects of lattice temperature on the physical quantities, such as electrostatic potential, electron and current densities, are investigated using TFA for the self consistent calculation. According to these results, the electron temperature is

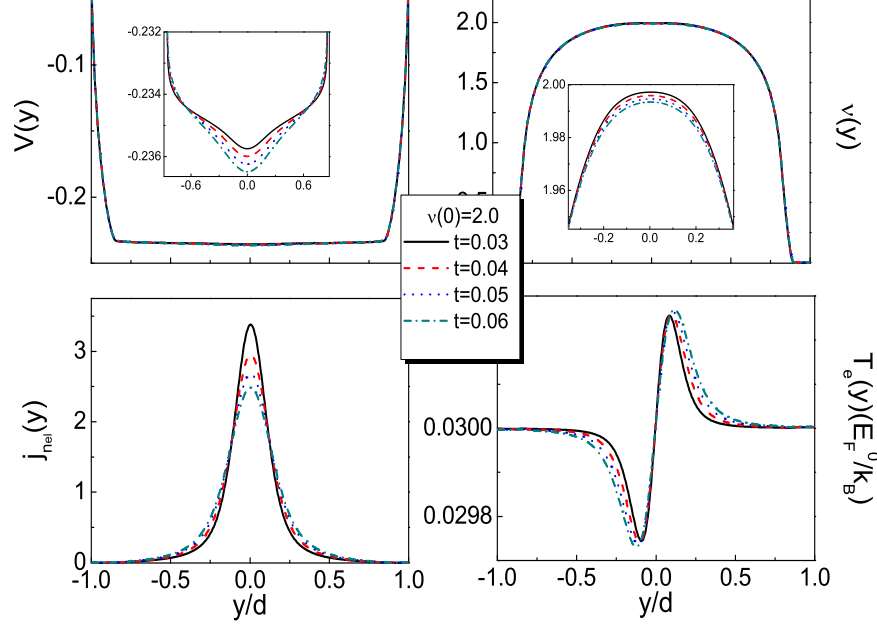


Figure 5.1 (a) Electrostatic potential $V(y)$, (b) filling factor $\nu(y)$, (c) current density $j_{nel}(y)$ and (d) electron temperature $T_e(y)$ at three temperatures, $t = k_B T_L / E_F^0$. The density of donor $n_0 = 3.6 \times 10^{11} \text{ cm}^{-2}$ and Hall bar of width $2d = 1 \mu\text{m}$ at the center of the filling factor $\nu(0) = 2.0$.

obtained for different lattice temperatures. The temperature effect on the calculated filling factor for the magnetic field 1.0, measured in units of $\hbar\omega_c / E_F^0$ ($\hbar\omega_c \equiv \Omega_c$) with $E_F^0 = 10.81 \text{ meV}$ is shown in Fig. 5.1, considering a $1 \mu\text{m}$ wide sample. With the center filling factor $\nu(0) = 2.0$, the potential shows non-linear spatial variations. As it is known, the dependence of the potential profile on the filling factor already suggests the important role of the electron-electron interactions, leading to finite widths of both compressible and incompressible strips. This figure shows that, when the $\nu(0)$ becomes very close to two, the two IS(s) merge at the bulk and all the current flows from the incompressible bulk. And also the electron temperature deviation with the non-linear potential is shown in Fig. 5.1. It shows the oscillating pattern reflecting the relative position of the electrochemical potential to the Landau levels. There exist the peak and dip structures in the electron temperature located near $y/d = \pm 0.1$.

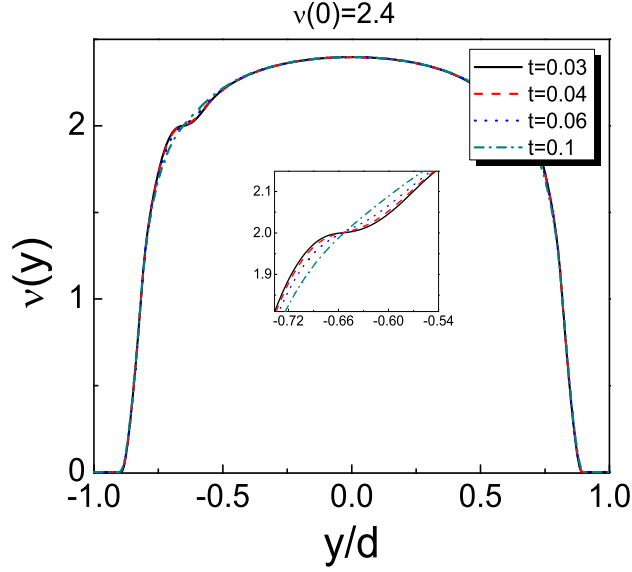


Figure 5.2 Filling factor $v(y)$ versus position for four values of the lattice temperature, $k_B T_L/E_F^0 = 0.03, 0.04, 0.06$ and 0.1 . Hall bar of width is $2d = 1\mu\text{m}$ and the magnetic field is $\Omega_c/E_F^0 = 0.83$. The inset shows the plateau region.

In Fig. 5.2, the spatial variation of the filling factor is plotted considering four different lattice temperatures. The magnetic field B strength is fixed as $\Omega_c/E_F^0 = 0.83$, where the bulk filling factor $v(0)$ is above 2. Here, Fermi energy at the bulk is calculated to be 10.81 meV. At the highest lattice temperature ($k_B T_L/E_F^0 = 0.1$), the electronic system is in a pure compressible state since both the lowest and next Landau levels are partially occupied due to the fact that the thermal energy of the electrons exceed the Landau gap. Therefore, no IS(s) are formed. Once lowering the temperature, it is observed that density distribution presents plateaus (i.e. is constant within a finite spatial interval) at opposing edges, which are the expected IS(s), where Fermi energy falls within the Landau gap locally hence, screening is poor and electrons cannot be redistributed. For the lowest lattice temperature, the IS(s) become even larger and stable.

If the spatial distributions of the electrostatic and electrochemical potentials are

known, the electron temperatures can be obtained. In the following results, the electron temperature is obtained starting from the results of the screening theory. Note that, the imposed current is assumed to be sufficiently small to guarantee that system is still within the linear response regime, hence, both the induced potential and the variations of the local electron temperature do not influence the electronic distribution.

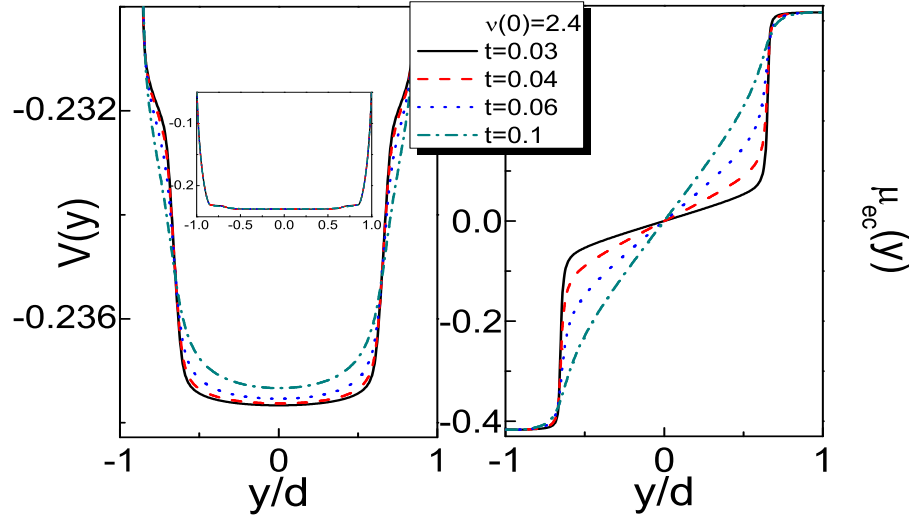


Figure 5.3 Calculated potential $V(y)$ and electrochemical potential $\mu_{ec}(y)$ versus position at four lattice temperature, $t = k_B T_L / E_F^0$. ($2d = 1 \mu\text{m}$, $\Omega_c / E_F^0 = 0.83$ and $\nu(0) = 2.4$).

Next the electrostatic and electrochemical potentials are obtained for the center filling factor $\nu(0) = 2.4$. The existence of the ISs is related to the gap between adjacent broadened LL's, provided that the temperature is low enough. With decreasing temperature, 2DES develops IS(s) with low longitudinal resistivity and the current density is increasingly confined to the incompressible regions. In the other words, the width of ISs increases monotonically and it has apparently a finite width for $T \rightarrow 0$. At the highest temperature ($T_L = 0.1 E_F^0 / k_B$) Drude-like behavior is observed. As it is shown in Fig. 5.3, electrochemical potential increases nearly linearly across the 2DES.

The electron temperature variation as a function of spatial coordinate is shown in

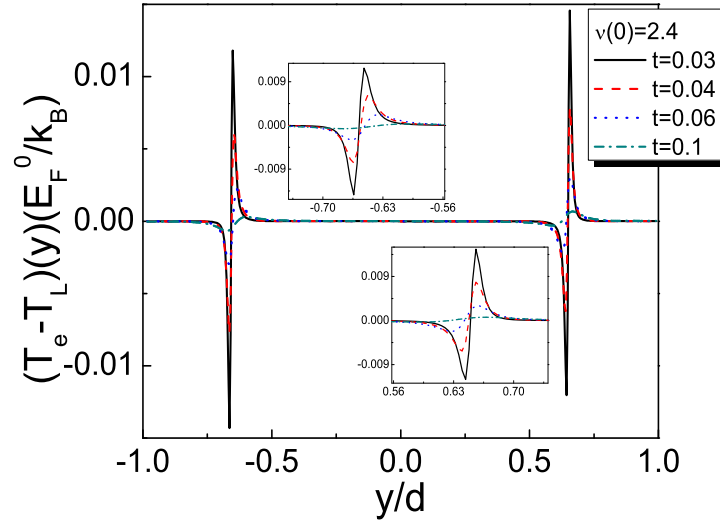


Figure 5.4 Spatial distributions of the electron temperature $T_e - T_L$ for several values of lattice temperature, $t = k_B T_L / E_F^0$. The insets show the variations of the electron temperature enlarged for both sides of the sample. ($2d = 1\mu\text{m}$, $\Omega_c / E_F^0 = 0.83$ and $v(0) = 2.4$).

Fig. 5.4, where the electron and potential profiles are shown in Figs. 5.2 and 5.3. As it is shown, assuming a higher lattice temperature results in small variations at the local electron temperature. This is expected, since at higher temperatures the IS(s) are not well developed, hence, current is spread all over the sample. Therefore, heating effects take place almost at the entire sample. Most interestingly, one observes that one side of the sample heats up, whereas the opposing edge is cooled down. This effect is nothing but the Peltier effect (Ahlsweide, Weitz, Weis, Klitzing, & Eberl, 2001; Ahlsweide, Weis, Klitzing, & Eberl, 2002). Although there is no net charge transfer in the y direction the thermal flux is transferred by the conservation of energy. Lowering the lattice temperature yields stronger IS(s), hence, current is more confined to these regions. As a direct consequence, the local electron temperature starts to vary stronger.

The calculated result of the current density $j(y)$ is given in Fig. 5.5. According to

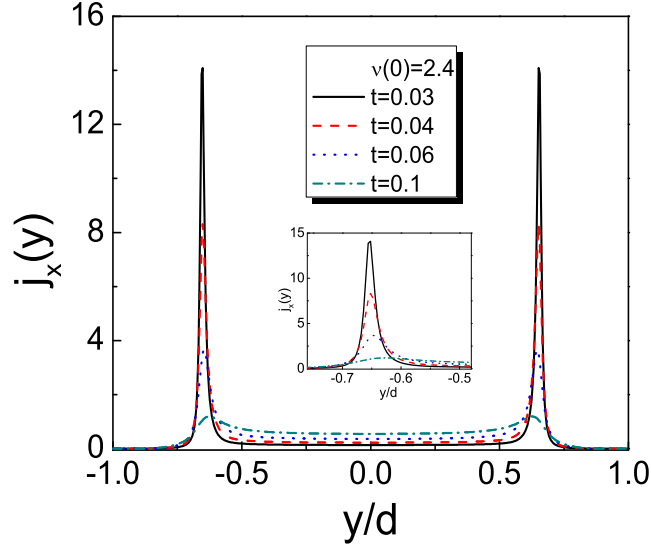


Figure 5.5 Spatial distributions of the current density $j_x(y)$ at four lattice temperature, $t = k_B T_L / E_F^0$. The inset shows the incompressible strip enlarged for the left side of the sample. ($2d = 1 \mu\text{m}$, $\Omega_c / E_F^0 = 0.83$ and $\nu(0) = 2.4$).

Ohm's law, $\Delta j_x = E_x / \rho_{xx}$ with ρ_{xx} longitudinal resistivity and the amplitude of current density depends on the value of $1/\rho_{xx}$. When μ_{ec} exists between two Landau levels, ρ_{xx} becomes small, therefore j_x increases. The peaks observed in ISs are same since T_L is uniform in the system. However at lowest T_L , the peaks are large and narrow. With increasing the T_L , the peaks become smaller and wider. At sufficiently high T_L , j_x spreads in 2DES since ISs disappear.

5.2.2 Magnetic Field Dependence

Now the effect of magnetic field on the electron temperatures is calculated for different values of magnetic field. Fig. 5.6 shows density profiles, electrostatic and electrochemical potentials obtained for four different magnetic fields at low temperature, $k_B T_L / E_F^0 = 0.03$. At sufficiently large B with the local filling factor $\nu(y) < 2$, the 2DES is completely compressible. For the lower B with the local filling factor

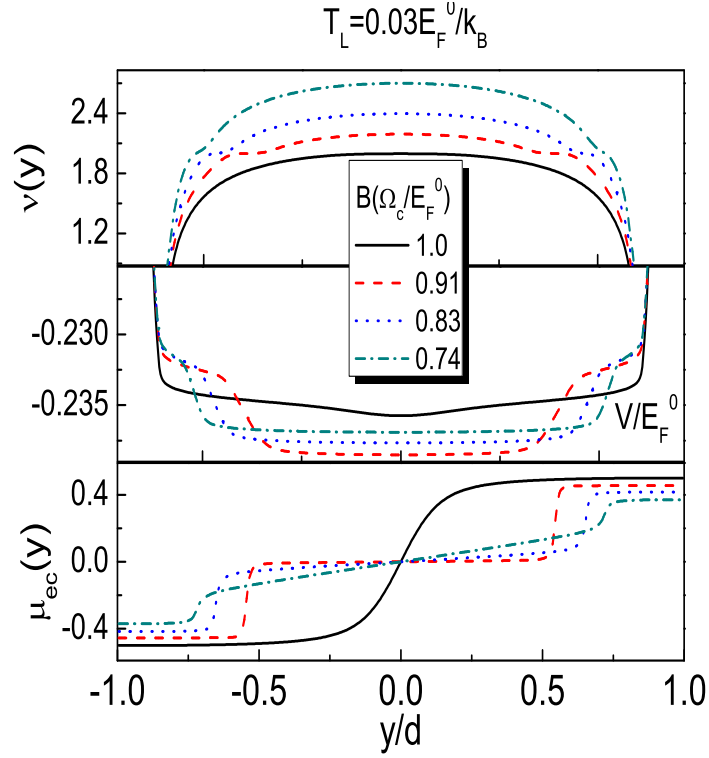


Figure 5.6 Calculated filling factor, electrostatic and electrochemical potentials for different magnetic fields, Ω_c/E_F^0 . The sample parameters are $2d = 1\mu\text{m}$, $n_0 = 3.6 \times 10^{11}\text{cm}^{-2}$ and $k_B T_L/E_F^0 = 0.03$.

$\nu(y) = 2$, the center of the sample becomes incompressible, while $\nu(y)$ gradually decreases outside the incompressible center and falls off to zero in the depletion regions at the sample edges. When B is decreased, the center filling factor increases and IS with $\nu(y) = 2$ move towards the sample edges and become narrower. This effect is seen clearly for low enough lattice temperature.

In this study the variation of T_e in y direction is considered, since T_e is uniform in x direction. In the linear response regime, T_e is proportional to the current density in QHS depending on compressible and incompressible strips. Fig. 5.7 shows the magnetic field dependence of T_e . The results for the lattice temperature $T_L = 0.03 E_F^0/k_B$ at $B = 1.0, 0.91, 0.83$ and $0.74 \Omega_c/E_F^0$ are shown in Fig. 5.7. It is seen that the electron temperature T_e shows spatially antisymmetric behavior that is obviously relevant to the

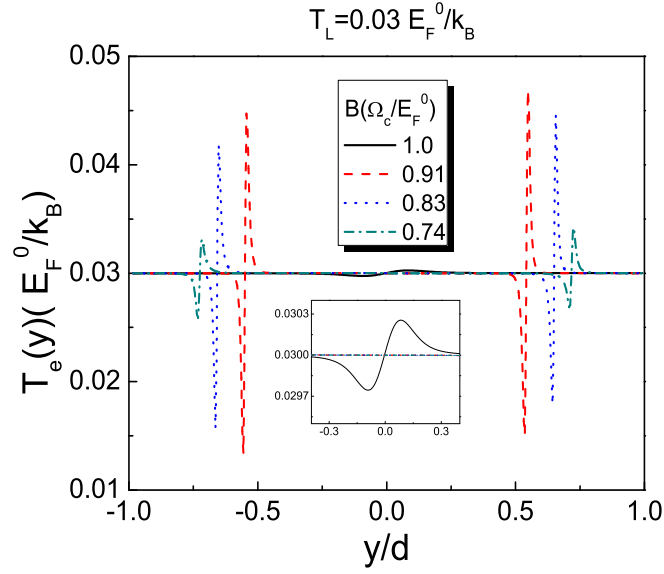


Figure 5.7 Spatial distributions of the electron temperature $T_e(y)$ for different values of magnetic field, $\Omega_c/E_F^0 = 1.0, 0.91, 0.83$ and 0.74 .

thermal flux in the y direction. Especially, transport coefficient including gradient of the electrochemical potential $\nabla\mu_{ec}$ is effective. Therefore the direction of this thermal flux is defined by the transport coefficient L_{xx}^{12} . Also it is shown that, the spatial dependence of the electron temperature strongly depends on magnetic field. The width of IS(s) decreases slowly with decreasing magnetic field since it is proportional to the magnetic field and ISs approach the sample edge. ISs become wider and move away from the sample edges with increasing the magnetic field.

Fig. 5.8 shows the spatial distribution of current densities for different magnetic field values. The sample width is $2d = 1 \mu\text{m}$. Data are shown for $T_L = 0.03 E_F^0/k_B$ as well as four values of the magnetic field ($\Omega_c/E_F^0 = 0.1, 0.91, 0.8$ and 0.74). Since spatial distribution of T_e varies strongly in ISs, the peaks are observed in these strips for different magnetic field, as shown in Fig. 5.8. As known, width and position of ISs change with different magnetic field values. This is the reason why, these peaks are located at different positions and have different magnitude in y direction corresponding

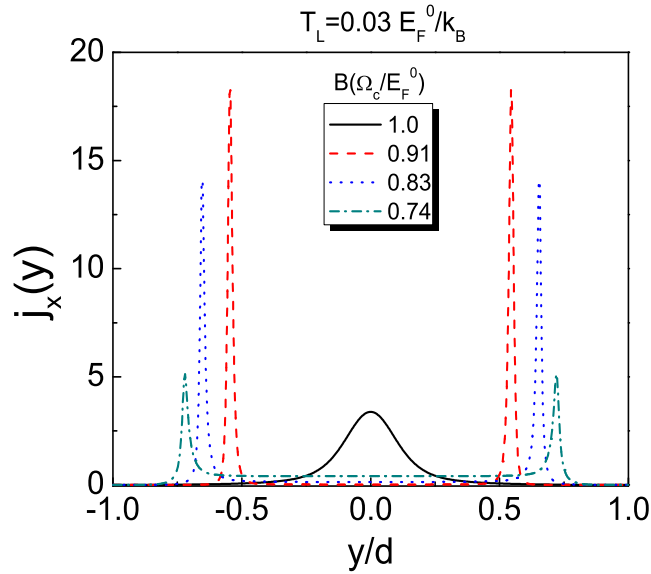


Figure 5.8 Spatial distributions of the current density $j_x(y)$ for different values of magnetic field, $\Omega_c/E_F^0 = 1.0, 0.91, 0.83$ and 0.74 at fixed lattice temperature, $T_L = 0.03 E_F^0/k_B$.

to ISs. For smaller B values, the ISs shrink and finally vanish, and the current density expands in 2DES. As a result, it is shown that the current densities are observed in ISs corresponding to the magnetic field values.

5.2.3 Sample Parameter Dependence

In QHS, the spatial distribution of electron temperature does not only depend on the magnetic field or the lattice temperature, but also on the sample parameters, such as sample width d , depletion length b and averaging length λ , since these parameters affect the width of the ISs. The effect of the sample width on the variation of electron temperature is indicated in Fig. 5.9. Here three sample widths, $2d = 1.6, 2.4$ and $3.0 \mu\text{m}$ are used with fixed magnetic field $\Omega_c/E_F^0 = 0.8$ and lattice temperature $T_L = 0.05 E_F^0/k_B$. With increasing the sample width, the strips move towards the sample edges and become narrower. Thus, the deviation of electron temperature $T_e - T_L$ increases

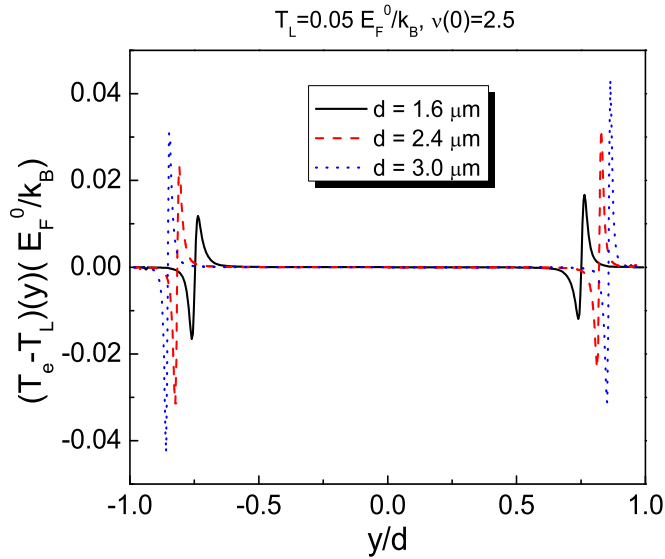


Figure 5.9 Spatial distributions of $(T_e - T_L)$ for different values of sample widths, $2d = 1.6, 2.4$ and $3.0 \mu\text{m}$. The lattice temperature $T_L = 0.03 E_F^0/k_B$ and magnetic field $\Omega_c/E_F^0 = 0.8$.

and moves from the center towards the sample edges.

The influence of averaging length is investigated for a magnetic field value corresponding to the central filling factor $\nu(0) = 2.4$. The effect of averaging length on the local filling factor $\nu(y)$ and electron temperature is demonstrated in Figs. 5.10 and 5.11. Fig. 5.10 shows that the averaging length yields changes in the width of the ISs at the lattice temperature $T_L = 0.04 E_F^0/k_B$ and fixed magnetic field, $\Omega_c/E_F^0 = 0.83$. With increasing the averaging length, ISs becomes narrower. This affects the variation of electron temperature depending on ISs. The result shows that with increasing λ , only the value of T_e changes, but the position is constant in y direction.

The no electron region is called depletion region and the electron density is affected by the depletion length, b . For the narrow depletion length the bulk density profile is nearly flat, whereas for the wide depletion length a bending profile is observed. These affect the existence of the ISs. Fig. 5.12 shows the deviation of electron tempera-

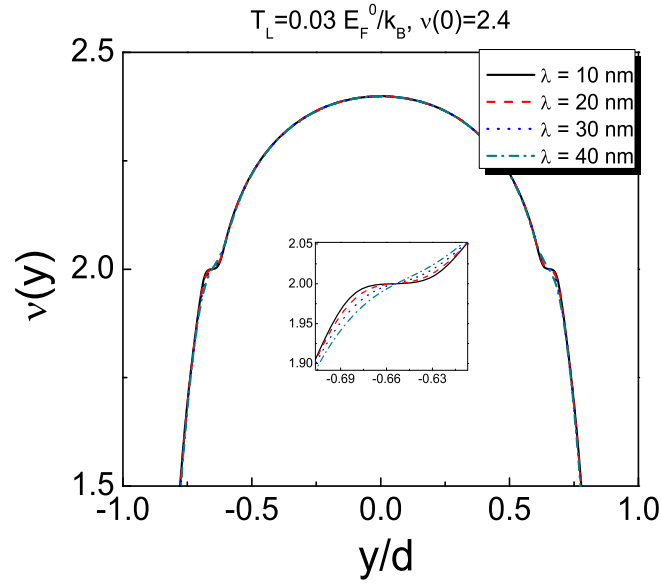


Figure 5.10 Filling factor profile for different values of the averaging length λ with the magnetic field $\Omega_c/E_F^0 = 0.83$. The sample parameters are $2d = 2 \mu\text{m}$, $n_0 = 4.0 \times 10^{11} \text{cm}^{-2}$ and $k_B T_L/E_F^0 = 0.04$.

ture for different values the depletion length, $b = 80, 100, 150, 200$ and 250 nm. With decreasing the depletion length, the deviation of electron temperature $T_e - T_L$ also decreases and moves from the center towards the sample edges.

5.3 Effects of the Energy Loss on the Electron Temperature

The results discussed in this section are calculated considering the energy loss that is given in Eq. 4.3.72. In this equation, a coupling between electrons and phonons is represented by C_p^0 . The electron temperature deviations are shown in Fig. 5.13 for different values of C_p^0 at (a) $v(0) = 2.0$ and (b) $v = 2.5$. The solid, dash, dot and dash dot lines represent the results for $C_p^0 = 3 \times 10^{-3}$, 5×10^{-2} and 8×10^{-2} . $k_B(E_F^0)/\hbar$ is used for scaling the coefficient. The lattice temperature is $T_L = 0.15E_F^0/k_B$ with $E_F^0 = 9.615$ meV. The variation of the electron temperature without electron phonon interaction is

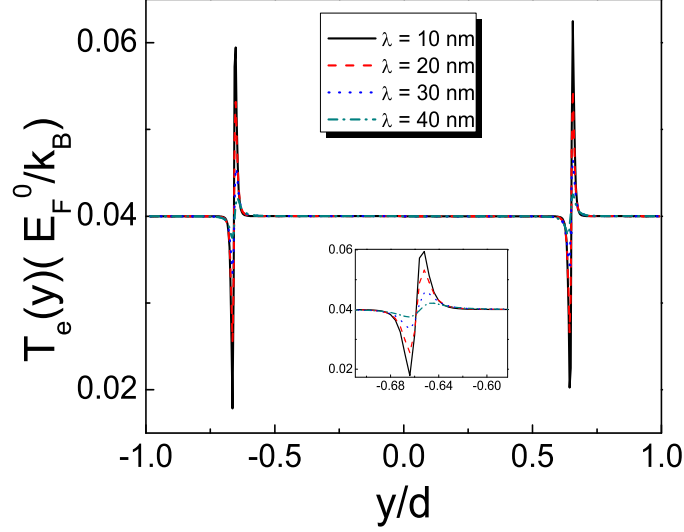


Figure 5.11 Spatial distributions of the electron temperature $T_e(y)$ for different values of the averaging length λ with the magnetic field $\Omega_c/E_F^0 = 0.83$ at fixed lattice temperature, $T_L = 0.04 E_F^0/k_B$. The inset shows the variation of T_e enlarged for the left side of the sample.

larger than the variation of the electron temperature with the interactions. Since a part of the energy is converted to the heat energy between electrons and phonons because of the interaction. With introducing the interaction, the heat transfer occurs between electron-phonons. So that C_p^0 coefficient reduces $|T_e - T_L|$. In the strong interaction limit between electrons and phonons, i.e. C_p^0 coefficient is infinite, $|T_e - T_L| = 0$. It is obtained that $|T_e - T_L|$ decreases with increasing the coefficient. This effect is clearly shown in the vicinity of the peak and dip structure at $y/d \approx \pm 0.37$ for $v(0) = 2.0$ and at $y/d \approx \pm 0.6$ for $v(0) = 2.5$.

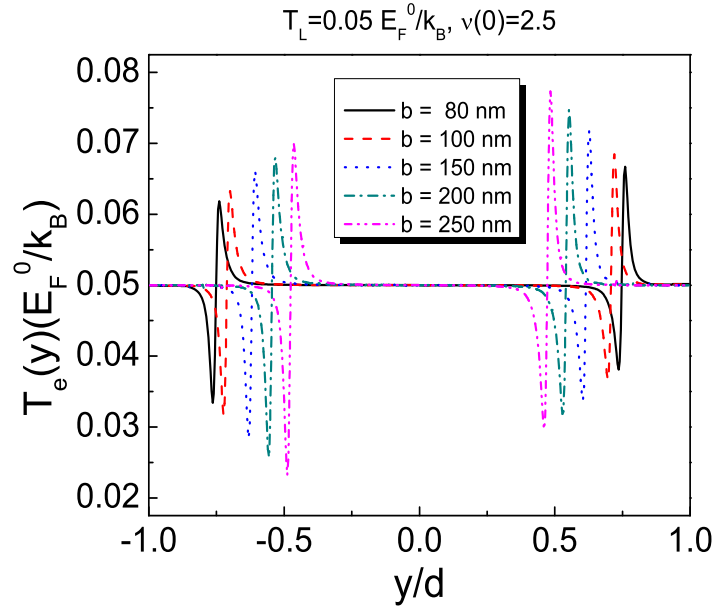


Figure 5.12 Spatial distributions of the electron temperature $T_e(y)$ for different values of depletion length, $b = 80, 100, 150, 200$ and 250 nm with $\Omega_c/E_F^0 = 0.8$. The sample parameters are $2d = 1.6 \mu\text{m}$, $n_0 = 4.0 \times 10^{11} \text{cm}^{-2}$, $\lambda = 33$ nm and $k_B T_L/E_F^0 = 0.05$.

5.4 Effects of the Electron Temperature on the Compressible and the Incompressible Strips

The changes in the local electron temperature T_e with increasing filling factor at fixed lattice temperature $T_L = 0.03 E_F^0/k_B$ are presented in Fig. 5.14. This figure shows that the electron temperature oscillates as a function of the lattice temperature in the ISs. And also it indicates that, the electron temperature strongly depends on the filling factor. The ISs shrink slowly with increasing the filling factor since it is inversely proportional to the filling factor and ISs approach the sample edges.

In Fig. 5.15, the filling factor and the current density profiles are compared for the temperature and electron temperatures. In the filling factor figure, where the lattice temperature is taken into account, ISs are same since T_L is uniform in the system.

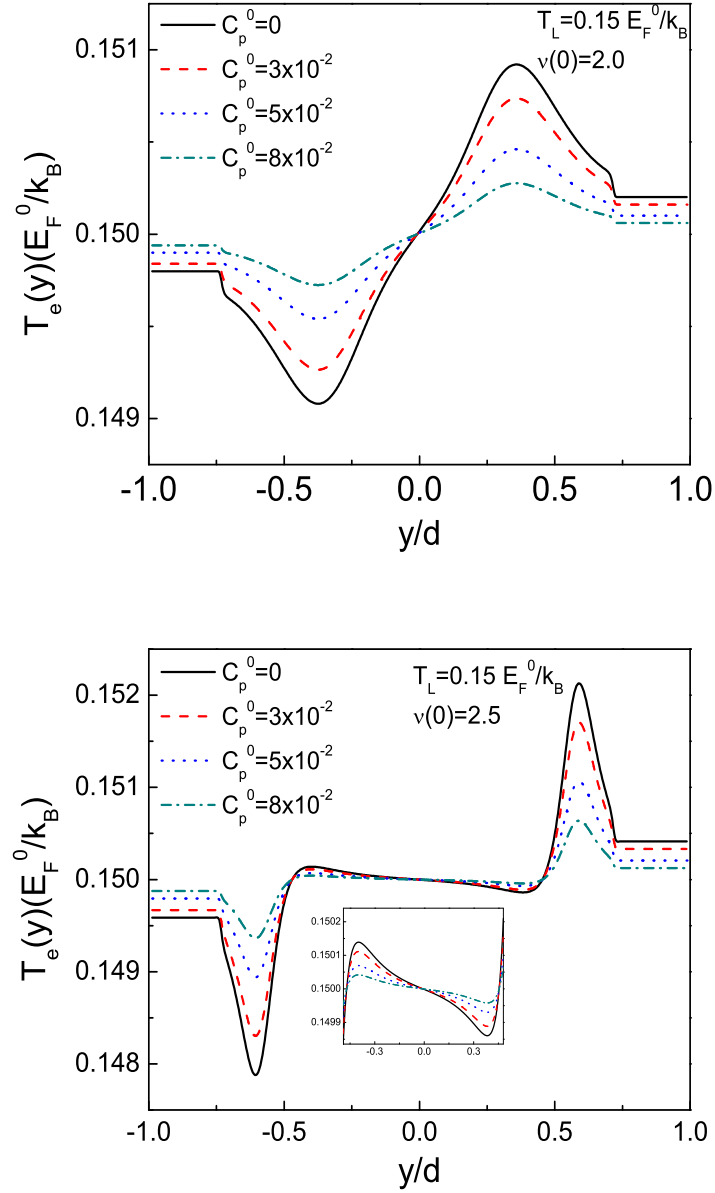


Figure 5.13 The electron temperature versus position, calculated for different center filling factor at fixed lattice temperature $T_L = 0.15 E_F^0/k_B$. The sample parameters are $2d = 2.2 \mu\text{m}$, $n_0 = 3.6 \times 10^{11} \text{cm}^{-2}$ and the Fermi energy $E_F^0 = 9.62 \text{meV}$ corresponding to the electron density at the center.

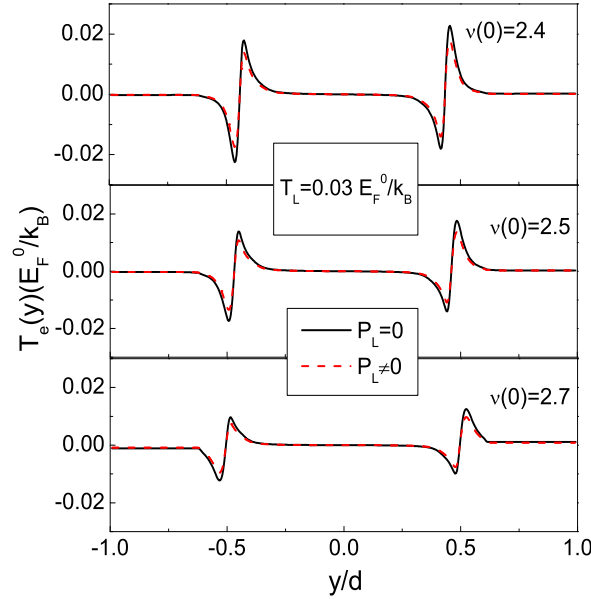


Figure 5.14 The electron temperature versus position, calculated for $\nu(0) = 2.4$ at fixed lattice temperature $T_L = 0.03 E_F^0/k_B$. The black and red lines represent the results for the without energy loss and with energy loss, respectively.

If the electron temperature is used to calculate the filling factor, the quantum Hall plateaus show different behavior. Since right side of the sample heats up, while the left side of the sample is cooled down. This effect is more evident at $\nu(0) = 2.4$, so we show the results for $\nu(0) = 2.4$. As expected, the width of the incompressible strip increases monotonically with decreasing temperature.

The result shows that when the electron temperature becomes smaller than the lattice temperature (left side), the 2DES develops IS(s) with low longitudinal resistivity and the current density is increasingly confined to the IS(s). Therefore in the left side of the sample, the red peak is larger than the black one. The other side of the sample is opposite.

In Fig. 5.16, the energy loss a positive P_L is considered in order to investigate the filling factor and current density profile using the electron temperature. As expected,

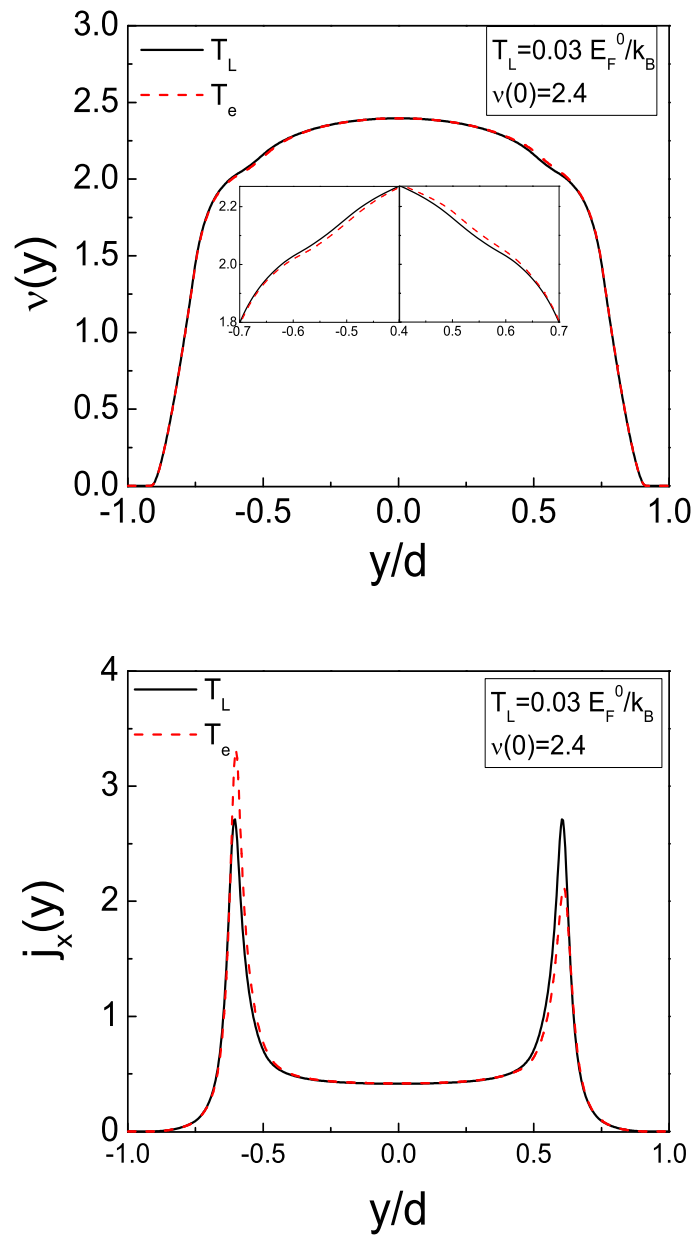


Figure 5.15 The filling factor and current density versus position for $\nu(0) = 2.4$ at fixed lattice temperature $T_L = 0.03 E_F^0/k_B$. The insets show the enlarged plateau regions (incompressible strips). For calculations we use the lattice temperature (black lines) and the electron temperature (red lines).

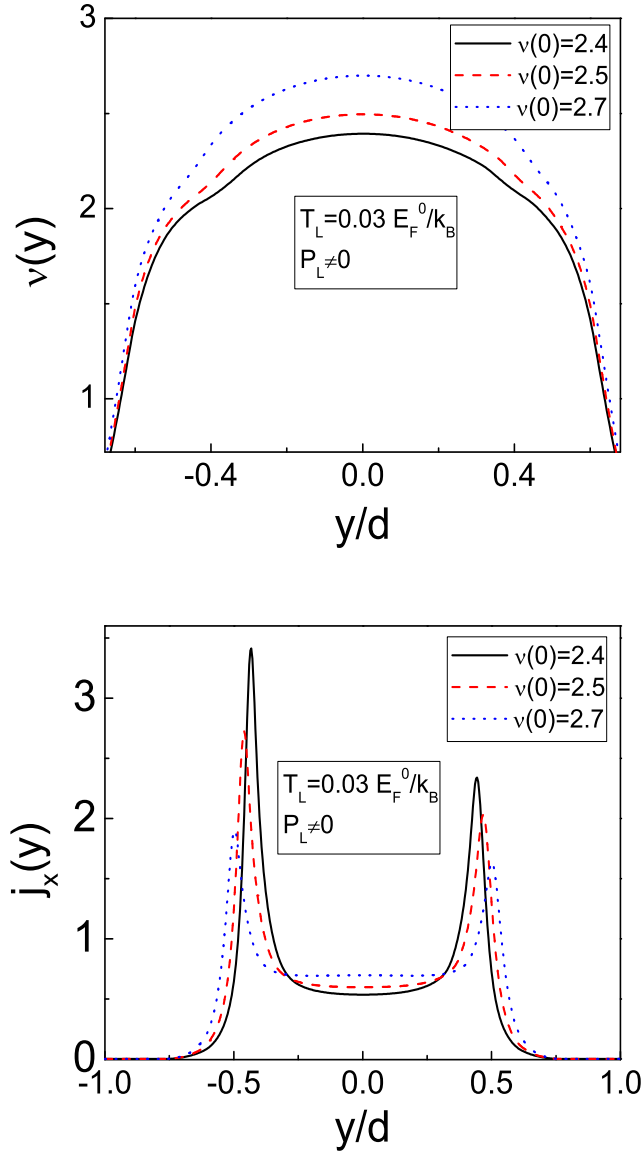


Figure 5.16 The filling factor and current density versus position for $\nu(0) = 2.4, 2.5$ and 2.7 at fixed lattice temperature $T_L = 0.03 E_F^0/k_B$.

with increasing the central filling factor, the quantum Hall plateaus become smaller and move from the center towards the edges. But depending on the electron temperature, incompressible strip that occurs at the right side of the sample becomes narrow for each central filling factor. Since at the right side of the sample, the electron temper-

ature becomes larger than the lattice temperature. As known, the width of the quantum Hall plateaus decreases with increasing the temperature. Also the current density is dependent on this effect. Therefore the difference between two ISs are shown for each center of the filling factor. This difference is larger at $\nu(0) = 2.4$, since the variation of electron temperature is much bigger, as it is seen from Fig. 5.14. The variation of the electron temperature becomes smaller at $\nu(0) = 2.7$, so the difference between two ISs nearly disappears.

CHAPTER SIX

TEMPERATURE DEPENDENT BREAKDOWN OF THE QUANTUM HALL RESISTANCE

6.1 Introduction

In Hall measurements on high mobility, two dimensional electron gas samples the resistance at the quantized plateaus is given by $R_H = h(\nu e^2)$. The resistivity of a material is usually determined by its intrinsic properties, however, these properties might also depend on the external parameters such as temperature T , external magnetic field B etc. Moreover, if the sample is subject to a perpendicular B field and the transverse resistivity (namely the Hall resistivity) is measured, one can also determine the type and the number density of the charge carriers. The Hall resistivity is linear in B for a typical three-dimensional materials, which is drastically altered at two-dimensional systems to a stepwise behavior. However in some samples and for special temperatures the resistance increases with increasing magnetic field to a value above that of the quantized plateau before it returns and stabilizes at $h/(\nu e^2)$ (Wang et al., 2000). This is called quantum Hall resistance overshoot in which the transverse resistivity exhibits an unusual behavior.

Resistance overshoot is experimentally investigated in relatively narrow samples and the results are discussed in the context of interaction induced IS(s) in a phenomenological manner (Sailer, Wild, Lang, Siddiki, & Bougeard, 2010). If a 2DES is subject to a perpendicular B field, by the virtue of Landau quantization and direct Coulomb interactions, the electronic system is composed of compressible and incompressible strips. The Fermi energy is pinned to one of the Landau levels at the compressible regions and falls in between quantized levels at the incompressible regions (Chklovskii et al., 1992). Note that the local filling factor $\nu(y) = 2\pi l^2 n_{el}(y)$ is an integer at the incompressible strips, where $l = \sqrt{\hbar/eB}$ is the magnetic length and $n_{el}(y)$ is the local electron number density. These co-existing strips change the intrinsic properties (e.g. screening, conductivity) of the electronic system considerably (Lier, &

Gerhardt, 1994). The compressible regions behave like a metal, due to high density of states (locally), whereas the incompressible can be considered as insulators. The existence and transport properties of these regions strongly depend on the temperature and B mainly, among other system parameters (Siddiki, & Gerhardt, 2004).

6.2 Model and Results

The Hall bar is considered as a 2DES in the plane $z = 0$, with translation invariance in the x direction and electron density $n_{\text{el}}(y)$ confined to the interval $-d < y < d$. The confinement potential $V_{\text{bg}}(y)$ due to donor and Hartree potential V_{H} due to electrons are given in Chapter 3. The solution involves the self-consistent determination of the electron density via

$$n_{\text{el}}(y) = \int dE D(E) f(E + V(y) - \mu^*) \quad (6.2.1)$$

which is valid in the approximation of a slowly-varying potential, the namely TFA. The density of states $D(E)$ is to be taken from self-consistent Born approximation (Ando, Fowler, & Stern, 1982) and μ^* is the constant equilibrium electrochemical potential. Since, the overshoot effect is independent of the actual origin of the single particle gap, from now on we assume spin degeneracy and neglect Zeeman splitting. DOS and local conductivities are determined assuming an impurity potential having a Gaussian form (Ando, Fowler, & Stern, 1982)

$$V(r) = \frac{V_I}{\pi R^2} \exp\left(-\frac{r^2}{R^2}\right), \quad (6.2.2)$$

where the range R is of the order of the spacing between 2DES and doping layer, together with the impurity strength V_I . In strong magnetic fields, the Landau levels are

broadened due to the scattering from the impurities and the level width is given by

$$\Gamma^2 = 4\pi n_I^2 V_I^2 / (2\pi l^2) = (2/\pi)\hbar\omega_c \hbar/\tau, \quad (6.2.3)$$

where n_I is the number density of the impurities and τ is the momentum relaxation time. We express the widths by the magnetic energy to characterize the impurity strength by the dimensionless ratio $\gamma = \Gamma/\hbar\omega_c$ and define the strength parameter as calculated at 10 T as

$$\gamma_I = [(2n_I V_0^2 m^* / \pi \hbar^2)(1.73 \text{ meV})]^{1/2}. \quad (6.2.4)$$

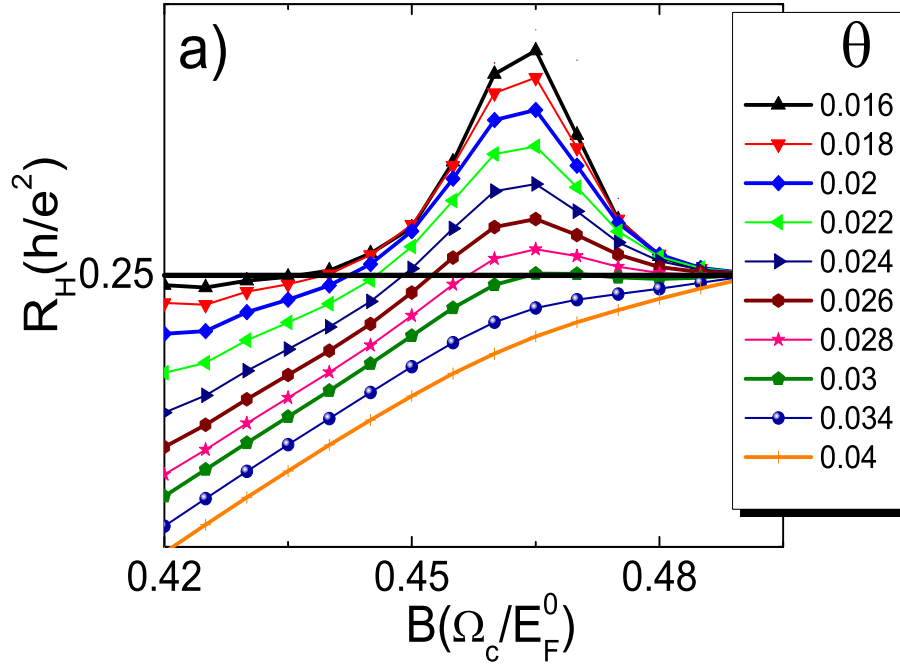


Figure 6.1 Magnetic field dependence of the Hall resistance R_H at different scaled temperatures $\Theta = k_B T/E_F^0$ with the sample width of $2d = 8 \mu\text{m}$, $\gamma_I = 0.3$.

The above set of equations allow us to determine the electron density, electrostatic potential and local conductivities in a self-consistent manner when solved numerically

by means of successive iterations.

In Figs. 6.1 and 6.2 Hall resistance as a function of B are shown where two different sample widths are used at various temperatures. One can clearly see the overshoot at the expected B intervals. The overshoot is smeared by the increase of the electron temperature, since the evanescent incompressible strip assuming $\nu = 2$ is washed out due to the condition $a_2 < l$. This finding also coincides with the experimental results showing that, the overshoot disappears with increasing temperature.

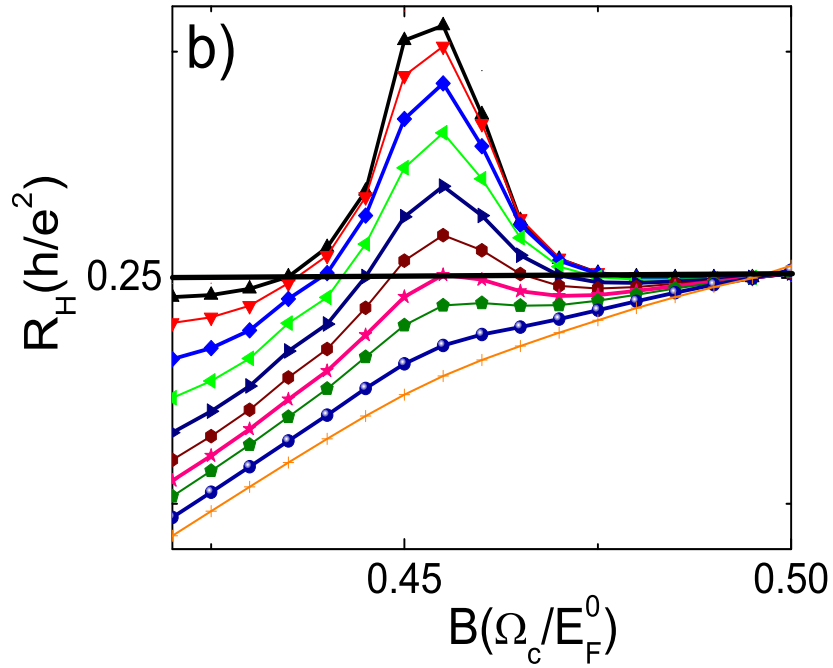


Figure 6.2 Magnetic field dependence of the Hall resistance R_H at different scaled temperatures $\Theta = k_B T / E_F^0$ with the sample width of $2d = 12 \mu\text{m}$, $\gamma_l = 0.3$.

Fig. 6.3 shows the effect of temperature on the overshoot in a more detailed manner in, considering a $10 \mu\text{m}$ wide sample and for three characteristic values of the B field. One sees that, the Hall resistance is impregnable to small temperature variations if the system is out of the overshoot regime (black solid line with boxes). Meanwhile at

the overshoot interval R_H depends strongly on the temperature, broken lines, which is even pronounced at the peak maximum.

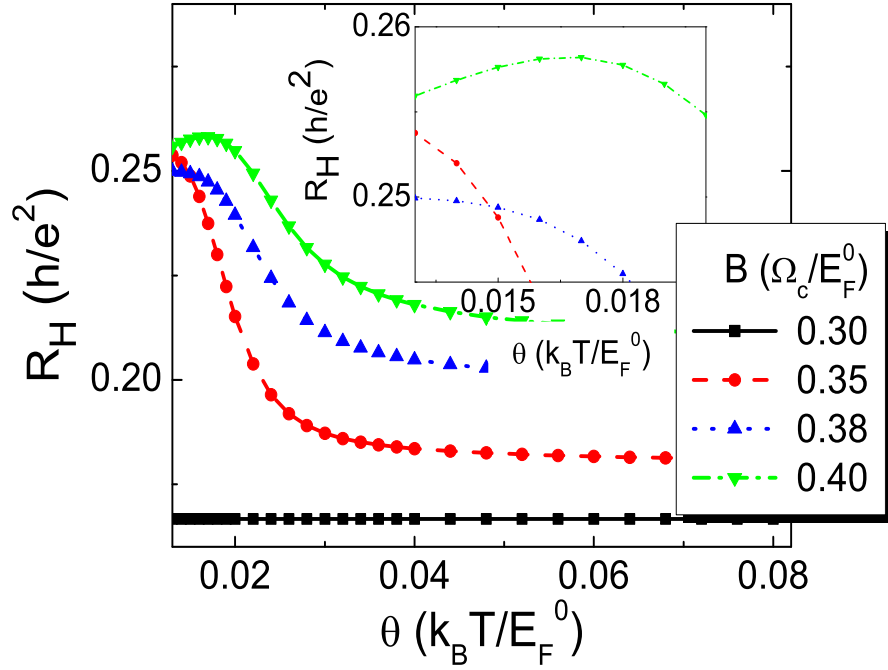


Figure 6.3 Calculated Hall resistance R_H versus scaled temperature (Θ), for different values of magnetic field, (Ω_c/E_F^0). The sample parameters are $2d = 10 \mu m$ and $\gamma_l = 0.05$.

6.3 Conclusion

In the light of above results and discussions we predict that, for the smooth edge defined samples the overshoot effect should be enhanced. The reason is: To have co-existing evanescent incompressible strips the condition $l < a_k, a_{k+1} < \lambda_F$ should be satisfied, this can only happen if the electron density varies slowly. Hence the strip becomes large. The experimental test can be as follows, one can define two narrow (e.g. $2d \sim 10 \mu m$) Hall bars residing parallel to each other, where one of the Hall bars is defined by shallow etching and the other by deep etching. Since, in principle, all the

intrinsic properties of the material would be the same for both samples the observed difference at the overshoots (enhanced at the shallow sample) would point out the effects due to the formation of wide evanescent incompressible strips. A gate defined sample can be utilized as well, similar to the ones reported in the literature (Horas, Siddiki, Moser, Wegscheider, & Ludwig, 2008).

CHAPTER SEVEN

CONCLUSION

The main aim of this thesis is to investigate spatial dependence of the electron temperature considering a 2DES under quantized Hall conditions when compressible and incompressible strips are formed. In order to obtain the electron temperature, thermohydrodynamic theory introduced by Akera et al. is used in linear response regime. This theory is described by equations of conservation with number and thermal flux densities.

The spatial distribution of the current density and electrochemical potential were calculated from a local version of Ohm's law. The electron density profile and electrostatic potential were obtained within a self-consistent TFPA to include classical electron-electron (Hartree) interaction. This approach is known as the screening theory of IQHE. In screening theory, heating effects are neglected since the electron temperature is assumed to be uniform through the system. In the other words, the electron temperature is taken into account as a lattice temperature.

In this thesis, one of the purposes is to calculate the spatial dependence of the electron temperature in IQHS, where compressible and incompressible strips are present as a result of interactions. The spatial distribution of the electron temperature was obtained by employing the theory of thermohydrodynamics that is bound by conservation of electron number and thermal flux densities, following Akera and his co-workers. This investigation differs from these pioneering works, as the realistic boundary conditions are performed. This leads to describing experimental systems accurately. Also this enables to predict an unexpected behavior that can be observed in the QHS based Aharonov-Bohm interference experiments, which is dictated by the local electron temperature variations.

The calculated results show that the current carried by the incompressible strips heats the electron system locally. Hence at low temperatures and at the low field

side of the quantized Hall plateau the heating is mainly local, whereas at the high field end of the plateau heating effect is spread all over the sample. This situation is altered at high lattice temperatures, since there are no well developed incompressible strips. Interestingly, one side of the sample heats up, whereas the opposite side is cooled down. From these observations, as expected, the edge-state transport is highly sensitive to formation of the incompressible strips. This leads to conclude that, even at low currents local heating effects may become important.

The other result discussed in the deviation of the electron temperature was calculated considering the energy loss. Energy loss represents a heat transfer due to electron-phonon scattering. Taking into account scattering in the linear response regime, the variation of the electron temperature becomes smaller than without the scattering. Since a part of the energy is converted to the heat energy between electrons and phonons because of the interaction.

Another purpose is to calculate the electron and current densities depending on the position in the presence of the electron temperature using the self-consistent TFPA. Nowadays, these quantities are investigated using the lattice temperature that is uniform in the system. Since in the linear response regime spatial variation of the electron temperature varies in the incompressible strips, the existence of electron temperature at quantizing magnetic fields at low lattice temperatures in 2DES changes the electron density profile and the spatial distribution of current density. The distributions of electron and current densities show that both side of the sample have symmetric plateau regions due to the uniform temperature. These plateau regions are modified with the electron temperature, since one side of the sample heats up, whereas the opposing edge is cooled down.

In summary, the electron temperature was indicated firstly for the realistic boundary conditions using the self-consistent TFPA. Thus, in QHS the experimental systems such as Aharonov-Bohm interference experiments can be described accurately.

Finally, effects of the electron temperature variation on distributions of the electron and current densities were discussed in the linear response regime.

Another interesting study is the quantum Hall resistance overshoot effect. The temperature and magnetic field effects on the overshoot resistance were investigated considering the GaAs/GaAlAs heterojunction. The results show that with increasing the temperature the overshoot peak decreases. The calculations show that the overshoot resistance as a function of magnetic field depends strongly on the edge electrostatics of the sample. Observation of enhanced resistance overshoot considering integer and fractional states is predicted by manipulating the edge potential profile.

REFERENCES

- Ahlsweide, E., Weitz, P., Weis, J., Klitzing, K. V., & Eberl, K. (2001). Hall potential profiles in the quantum Hall regime measured by a scanning force microscope. *Physica B*, 298 (1-4), 562-566.
- Ahlsweide, E., Weis, J., Klitzing, K. v., & Eberl, K. (2002). Hall potential distribution in the quantum Hall regime in the vicinity of a potential probe contact. *Physica E*, 12 (1-4), 165-168.
- Akera, H. (2000). Electronic processes at the breakdown of the quantum Hall effect. *J. Phys. Soc. Jpn.*, 69, 3174-3177.
- Akera, H. (2001). Hydrodynamic equation for the breakdown of the quantum Hall effect in a uniform current. *J. Phys. Soc. Jpn.*, 70, 1468-1471.
- Akera, H. (2002). Hydrodynamic equations in quantum Hall systems at large currents. *J. Phys. Soc. Jpn.*, 71, 228-236.
- Akera, H., & Suzuura, H. (2005). Thermohydrodynamics in quantum Hall systems. *J. Phys. Soc. Jpn.*, 74, 997-1005.
- Ando, T., Fowler, A. B., & Stern, F. (1982). Electronic properties of two dimensional systems. *Rev. Mod. Phys.*, 54 (2), 437-672.
- Ashcroft, N. M., & Mermin, N. D. (1984). *Solid State Physics*. Saunders College:Philadelphia.
- Boz Yurdasan, N., Akgungor, K., Siddiki, A., & Sokmen, I. (2012). Theoretical investigation of local electron temperature in quantum Hall systems. *Physica E*, (inprint).
- Cage, M. E., Dziuba, R. F., Field, B. F., Williams, E. R. , Girvin, S. M., Gossard, A. C., Tsui, D. C., & Wagner, R.J. (1983). Dissipation and dynamic nonlinear behavior in the quantum Hall regime. *Phys. Rev. Lett.*, 51, 1374-1377.

- Chklovskii, D. B., Shklovskii, B. I., & Glazman, L. I. (1992). Electrostatics of edge channels. *Phys. Rev. B*, *46* (7), 4026-4034.
- Chklovskii, D. B., Matveev, K. A., & Shklovskii, B. I. (1993). Ballistic conductance of interacting electrons in the quantum Hall regime. *Phys. Rev. B*, *47* (19), 12605-12617.
- Ebert, G., Klitzing, K. v., Ploog, K., & Weimann, G. (1983). Two-dimensional magneto-transport on GaAs-Al_xGa_{1-x}As heterostructures under non-ohmic conditions. *J. Phys. C: Solid State Phys.*, *16*, 5441-5448.
- Fowler, A. B., Fang, F. F., Howard, W. E., & Stiles, P. J. (1966). Magneto-oscillatory conductance in silicon surfaces. *Phys. Rev. Lett.*, *16* (20), 901-903.
- Gerhardts, R. R. (2008). The effect of screening on current distribution and conductance quantisation in narrow quantum Hall systems. *Physica Status Solid (b)*, *245* (2), 378-392.
- Griffin, N., Dunford, R. B., Pepper, M., Robbins, D. J., Churchill, A. C., & Leong, W. Y. (2000). Inter-edge-mode scattering in a high-mobility strained silicon two-dimensional electron system. *J. Phys.: Condens. Matter*, *12*, 1811-1818.
- Gurevich, A. V. & Mints, R. G. (1984). Nonlinear waves in the quantum Hall regime. *Soviet JETP Letters*, *39*, 381-382.
- Güven, K., Gerhardts, R. R., Kaya, I. I., Sağol, B. E., & Nachtwei, G. (2002). Two-level model for the generation and relaxation of hot electrons near the breakdown of the quantum Hall effect. *Phys. Rev. B*, *65* (15), 155316/1-8.
- Güven K., & Gerhardts, R. R. (2003). Self-consistent local equilibrium model for density profile and distribution of dissipative currents in a Hall bar under strong magnetic fields. *Phys. Rev. B*, *67* (11), 115327/1-8.
- Hall, E. H. (1879). On a new action of the magnet on electric currents. *American Journal of Mathematics*, *2*, 287-292.

- Horas, J., Siddiki, A., Moser, J., Wegscheider, W., & Ludwig, S. (2008). Investigations on unconventional aspects in the quantum Hall regime of narrow gate defined channels. *Physica E*, *40*, 1130-1132.
- Ise, T., Akera, H., & Suzuura, H. (2005). Electron temperature distribution and hot spots in quantum Hall systems. *J. Phys. Soc. Jpn.*, *74*, 259-262.
- Jeckelman, B., & Jeanneret, B. (2003). The quantum Hall effect as an electrical resistance standard. *Meas. Sci. Technol.*, *14*, 1229-1236.
- Kanamaru, S., Suzuura, H., & Akera, H. (2006). Spatial Distributions of Electron Temperature in Quantum Hall Systems with Compressible and Incompressible Strips. *J. Phys. Soc. Jpn.*, *75*, 064701.
- Karlhede, A., Kivelson, S. A., & Sondhi, S. L. (1992). *The quantum Hall effect*. University of California: Los Angeles.
- Kawaguchi, Y., Hayashi, F., Komiyama, S., Osada, T., Shiraki, Y., & Itoh, R. (1995). Disappearance of the breakdown of quantum Hall effects in short devices. *Jpn. J. Appl. Phys.*, *34*, 4309-4312.
- Kawaji, S., & Wakabayashi, J. (1976). Quantum galvanomagnetic properties of n-type inversion layers on Si(100) MOSFET. *Surf. Sci.*, *58*, 238-245.
- Kawaji, S., Hirakawa, K., & Nagata, M. (1993). Device-width dependence of plateau width in quantum Hall states. *Physica B*, *184*, 17-20.
- Kawaji, S., Hirakawa, K., Nagata, M., Okamoto, T., Fukuse, T. & Gotoh, T. (1994). Breakdown of the quantum Hall effects in GaAs/AlGaAs heterostructures due to current. *J. Phys. Soc. Jpn.*, *63*, 2303-2313.
- Kaya, I. I., Nachtwei, G., Klitzing, K. v., & Eberl, K. (1998). Spatial evolution of hot electron relaxation on quantum Hall conductors. *Phys. Rev. B-Rapid Comm.*, *58*, 7536.

- Kittel, C. (1953). *Introduction to Solid State Physics. (7th edition)*. Wiley:New York.
- Klitzing, K. v., Dorda, G., & Pepper, M. (1980). New Method for High-Accuracy Determination of the fine-structure constant based on quantized Hall resistance. *Phys. Rev. Lett.*, 45 (6), 494-497.
- Klitzing K. v. (1986). The quantized Hall effect. *Reviews of Modern Physics*, 58 (3), 519-531 .
- Komiyama, S., Takamasu, T., Hiyamizu, S., & Sasa, S. (1985). Breakdown of the quantum Hall effect due to electron heating. *Solid State Commun.*, 54, 479-484.
- Komiyama, S., Sakuma, H., Ikushima, K. & Hirakawa, K. (2006). Electron temperature of hot spots in quantum Hall devices. *Phys. Rev. B.*, 73, 045333/1-5.
- Kramer, B., Kettemann, S., & Ohtsuki, T. (2003). Localization in the quantum Hall regime. *Physica E*, 20, 172-187.
- Kuchar, F., Bauer, G., Weimann, G. & Burkhard, H. (1984). Non equilibrium behavior of the two-dimensional electron gas in the quantized Hall resistance regime of GaAs/Al_{0.3}Ga_{0.7}As. *Surf. Sci.*, 142, 196.
- Laughlin, R. B. (1981). Quantized Hall conductivity in two dimensions. *Phys. Rev. B*, 23, 5632-5633.
- Lier, K., & Gerhardts, R. R. (1994). Self-consistent calculations of edge channels in laterally confined two-dimensional electron systems. *Phys. Rev. B*, 50 (11), 7757-7767.
- Oh, J. H., & Gerhardts, R. R. (1997). Self-consistent Thomas-Fermi calculation of potential and current distributions in a to-dimensional Hall bar geometry. *Phys. Rev. B*, 56 (20), 13519-13528.
- Ramvall P., Carlsson N., Omling P., Samuelson L., Seifert, W., Wang, Q., Ishibashi, K. & Aoyagi, Y. (1998). Quantum transport in high mobility modulation doped Ga_{0.25}In_{0.75}As/InP quantum wells. *J. Appl. Phys.*, 84, 2112.

- Richter, C. A., Wheeler, R. G., & Sacks, R. N. (1992). Overshoot of quantum Hall plateaus. *Surf. Sci.*, 263, 270-274.
- Sagol, B. E. (2003). *Space and Time-Resolved Measurements at the Breakdown of the Quantum Hall Effect*. Technischen Universitt Carolo, Germany: Ph.D. Thesis.
- Sailer, J., Wild, A., Lang, V., Siddiki, A., & Bougeard, D. (2010). Quantum Hall resistance overshoot in two dimensional (2D) electron gases: theory and experiment. *New J. Phys.*, 12, 113033.
- Shlimak, I., Ginodman, V., Gerber, A. B., Milner, A., Friedland, K. J., & Paul D. J. (2005). Transverse "resistance overshoot" in a Si/SiGe two-dimensional electron gas in the quantum Hall effect regime. *Europhys. Lett.*, 69, 997-1002.
- Shlimak, I., Friedland, K.-J., Ginodman, V., & Kravchenko, S. (2006). Disorder-induced features of the transverse resistance in a Si-MOSFET in the quantum Hall regime. *phys. status solidi (c)*, 3 (2), 309-312.
- Siddiki, A. (2005). *Model Calculations of Current and Density Distributions in Dissipative Hall Bars*. Stuttgart: Ph.D. Thesis.
- Siddiki, A. (2007). Self-consistent Coulomb picture of an electron-electron bilayer system. *Phys. Rev. B*, 75 (15), 155311/1-15.
- Siddiki, A., & Gerhardts, R. R. (2003). Thomas-Fermi-Poisson theory of screening for laterally confined and unconfined two-dimensional electron systems in strong magnetic fields. *Phys. Rev. B*, 68 (12), 125315/1-12.
- Siddiki, A., & Gerhardts, R. R. (2004). Incompressible strips in dissipative Hall bars as origin of quantized Hall plateaus. *Phys. Rev. B*, 70 (19), 195335.
- Siddiki, A., & Gerhardts, R. R. (2004). The interrelation between incompressible strips and quantized Hall plateaus. *International Journal of Modern Physics B*, 18, 3541-3544.

- Siddiki, A., & Marquardt, F. (2007). Self-consistent calculation of the electron distribution near a quantum point contact in the integer quantum Hall effect. *Phys. Rev. B*, 75 (4), 045325/1-11.
- Stormer, H. L., Chang, A., Tsui, D. C., Hwang, J. C. M., Gossard, A. C. & Wiegmann W. (1983). Fractional quantization of the Hall effect. *Phys. Rev. Lett.*, 50 (24), 1953-1956.
- Stormer, H. L., Tsui, D. C., & Gossard, A. C. (1999). The fractional quantum Hall effect. *Rev. Mod. Phys.* 71, 298-305.
- Thouless, D. J., Kohmoto, M., Nightingale, M. P., & den Nijs, M. (1982). Quantized Hall conductance in a two-dimensional periodic potential. *Phys. Rev. Lett.*, 49, 405-408.
- Tsui, D. C., Störmer, H. L., & Gossard, A. C. (1982). Two-dimensional magnetotransport in the extreme quantum limit. *Phys. Rev. Lett.*, 48 (22), 1559-1562.
- Vasile, G. (2007). *Measurements and Modeling of the Dynamics of Optically and Electrically Induced Dissipation in Quantum Hall Systems*. Physik der Technischen Universität, Germany: Ph.D. Thesis.
- Wang, Q., Xu, H. Q., Omling, P., Yang, C, & Malmqvist, K. G. (2000). Defect-induced overshoot of quantum Hall plateaus. *Semicond. Sci. Technol.*, 15, 529-534.

APPENDIX A

A.1 Background (Free Electron Theory of Metals)

A.1.1 *Drude model*

The Drude model of electrical conduction was developed at the turn of the 20th century by Paul Drude to explain the transport properties of electrons in materials. Kinetic theory and Boltzmann distribution were used in Drude model and applied to the electrons in metals. It assumes that the material contains immobile positive ions and an “electron gas” of classical, non-interacting electrons of density, each of whose motion is damped by a frictional force, due to collisions of the electrons with the ions.

Drude achieved to explain the thermal as well as the electrical and optical properties of metals by the movement of electrons. He assumed that matter consists of free and bound electrons; conductors have a larger number of free electrons compared to insulator. The charge of the electrons is a multiple of the elementary charge; in fact, Drude was talking about positive and negative charged particles. The free electrons can be treated as particles of an ideal gas which all move with the same velocity. The kinetic energy is proportional to the temperature. The electrons are scattered at the ions. The electrical conductivity is proportional to the concentration of electrons, the mean free path, and inversely proportional to the mass and the velocity of the electrons.

A.1.2 *Electrical conductivity*

Based on the assumptions in Drude model and the application of kinetic theory, Ohm’s law can be driven. Consider a segment of a metal wire which includes a large number of electrons and has a uniform electric field. These electrons have different

speeds in different directions (Fig. A.1). The velocity of an electron between two collisions is defined by Newton's second law:

$$m \frac{d\mathbf{v}}{dt} = -e\mathbf{E}, \quad (\text{A.1.1})$$

where

$$\mathbf{v} = \mathbf{v}_0 - \frac{e}{m}\mathbf{E}t, \quad (\text{A.1.2})$$

with velocity after the last collision \mathbf{v}_0 and time elapsed from the last collision t . The average velocity is given by;

$$\langle \mathbf{v} \rangle = -\frac{e\tau}{m}\mathbf{E}, \quad (\text{A.1.3})$$

with the mean free time of the electrons τ .

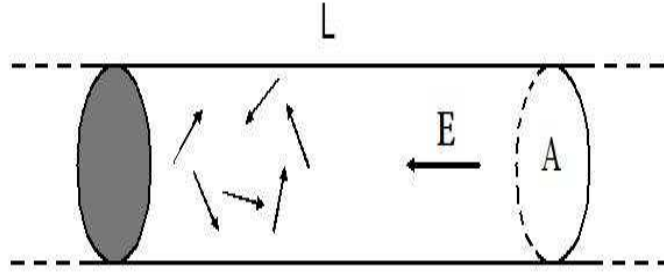


Figure A.1 Conduction in a metal wire.

This is a typical transport problem with \mathbf{v}_D proportional to the force. The mobility coefficient is $\mu_e = \tau/m$. The current density due to all the electrons in the wire is a sum over all the velocities;

$$\mathbf{J} = -e \sum_{\mathbf{v}} n(\mathbf{v})\mathbf{v} = -ne \langle \mathbf{v} \rangle, \quad (\text{A.1.4})$$

with the electron numbers per unit volume in the wire $n(\mathbf{v})$ and electron concentration n . The negative sign represents the negative charge of the electrons. Finally, the local form of Ohm's law is written;

$$\mathbf{J} = \sigma\mathbf{E}, \quad (\text{A.1.5})$$

with the electrical conductivity σ which is defined by;

$$\sigma = \frac{ne^2\tau}{m}. \quad (\text{A.1.6})$$

A.1.3 Thermal conductivity

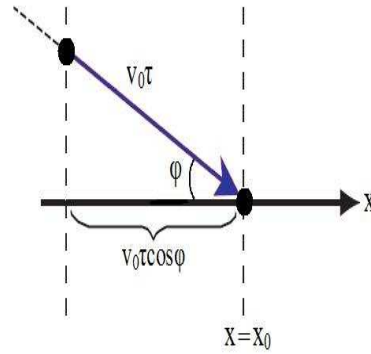


Figure A.2 An electron crossing the plane $x = x_0$ at an angle θ to the x-axis.

The thermal current depends upon temperature gradient ∇T and thermal conductivity of the material. If ∇T is nonzero, the average thermal energy which is given by $\frac{1}{2}mv_0^2$ depends on the local temperature $T(x)$. The thermal energy of an electron is related to the last collision. An electron crossing the plane $x = x_0$ at an angle θ to the x-axis has its last collision at $x = x_0 - v_0\tau \cos \theta$ and its energy $E(x) = E(x_0 - v_0\tau \cos \theta)$ (Fig. A.2). The number of such electrons crossing a unit area at x_0 is $nv_0 \cos \theta d\Omega/4\pi$ giving for the energy flux through a unit area at x_0 ;

$$j(x_0) = \int E(x_0 - v_0\tau \cos \theta)nv_0 \cos \theta d\Omega/4\pi \quad (\text{A.1.7})$$

while the energy is extended and the equation is integrated over θ from 0 to π , it becomes;

$$j(x) = -\frac{1}{3}nv_0^2\tau \left(\frac{\partial E}{\partial x} \right). \quad (\text{A.1.8})$$

Since $\frac{\partial E}{\partial x} = \frac{\partial E}{\partial T} \frac{\partial T}{\partial x}$ can be written, the thermal conductivity is given by;

$$\kappa = -\frac{j}{\partial T / \partial x} = \frac{1}{3} n v_0^2 \tau \frac{dE}{dT} = \frac{1}{3} v_0^2 \tau C_v, \quad (\text{A.1.9})$$

where C_v is the heat capacity per unit volume and is defined by

$$C_v = n \frac{dE}{dT}. \quad (\text{A.1.10})$$

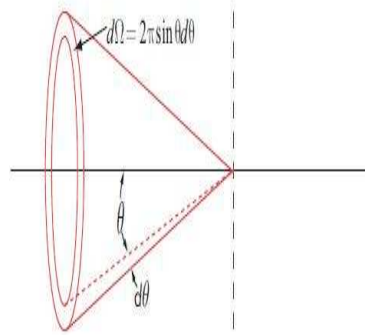


Figure A.3 Solid angle d in which electrons moving to cross the plane $x = x_0$ at an angle θ to the x -axis.

A.2 Wiedemann-Franz law

The Wiedemann-Franz law states that the ratio of the electronic contribution to the thermal conductivity κ and the electrical conductivity σ of a metal is proportional to the temperature T

$$\frac{\kappa}{\sigma} = \frac{\frac{1}{3} v_0^2 \tau C_v}{\frac{ne^2 \tau}{m}}. \quad (\text{A.2.1})$$

Drude applied the classical gas laws to evaluation of v_0^2 and C_v , $\langle \frac{1}{2} m v_0^2 \rangle = \frac{3}{2} k_B T$ and $C_v = \frac{3}{2} n k_B$. Then it gives

$$\frac{\kappa}{\sigma} = \mathcal{L} T, \quad (\text{A.2.2})$$

where \mathcal{L} is the proportionality constant, known as the Lorentz number, is equal to

$$\mathcal{L} = \frac{3}{2} \left(\frac{k_B}{e} \right)^2 = 1.24 \times 10^{-13} \text{ esu.} \quad (\text{A.2.3})$$

A.3 Thermoelectric Cooling and Heating

A thermoelectric cooler, sometimes called a thermoelectric module or Peltier cooler, is a semiconductor-based electronic component that functions as a small heat pump. By applying a low voltage DC power source to a thermoelectric cooler module, heat will be moved through the module from one side to the other. One module face, therefore, will be cooled while the opposite face simultaneously is heated. It is important to note that this phenomenon may be reversed whereby a change in the polarity (plus and minus) of the applied DC voltage will cause heat to be moved in the opposite direction. Consequently, a thermoelectric module may be used for both heating and cooling thereby making it highly suitable for precise temperature control applications.

The Seebeck, Peltier, and Thomson Effects, together with several other phenomena, form the basis of functional thermoelectric modules.

- *Joule heating*: Heating occurs in a conductor carrying an electric current. Joule heat is proportional to the square of the current, and is independent of the current direction.
- *Seebeck effect*: A voltage (Seebeck EMF) is produced in a thermoelectric material by a temperature difference. The induced voltage is proportional to the temperature difference. The proportionality coefficient is known as the Seebeck coefficient.
- *Peltier effect*: Cooling or heating occurs at the junction of two dissimilar thermoelectric materials when an electric current flows through the junction. Peltier

heat is proportional to the current, and changes sign if the current direction is reversed.

- *Thomson effect*: Heat is absorbed or released in a non-uniformly heated thermoelectric material when electric current flows through it. Thomson heat is proportional to the current, and changes sign if the current direction is reversed.

A.4 Fermi Dirac Distribution Function

At zero temperature, the Fermi Dirac distribution function can be written as a function of energy ϵ :

$$f(\epsilon) = \begin{cases} 1 & \epsilon < \epsilon_F \\ 0 & \epsilon > \epsilon_F \end{cases} \quad (\text{A.4.1})$$

where ϵ_F is Fermi energy. At a finite temperature, it is given by;

$$f(\epsilon) = \frac{1}{e^{(\epsilon - \epsilon_F)/k_B T} + 1} \quad (\text{A.4.2})$$

with the Boltzmann constant k_B . The Fermi Dirac distribution function is plotted in the figure below.

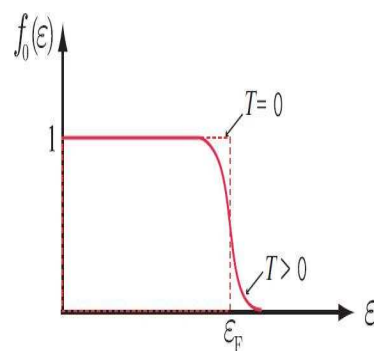


Figure A.4 Fermi Dirac distribution function at two different temperatures as a function of the energy.

A.5 Thermodynamic Potential

Thermodynamic potentials are used to measure the energy of a system in terms of different variables. The functions that are commonly used in statical mechanics are:

$$\textit{internal energy} \quad U,$$

$$\textit{Helmholtz free energy} \quad F = U - TS,$$

$$\textit{Thermodynamic potential} \quad \Omega = -PV,$$

$$\textit{Enthalpy} \quad H = U + PV,$$

$$\textit{Gibbs free energy} \quad G = U - TS + PV.$$

For the above functions, the fundamental equations are expressed as:

$$dU = TdS - PdV + \sum_i \mu_i dN_i, \quad (\text{A.5.1})$$

$$dF = -SdT - PdV + \sum_i \mu_i dN_i, \quad (\text{A.5.2})$$

$$dH = TdS + VdP + \sum_i \mu_i dN_i, \quad (\text{A.5.3})$$

$$dG = -SdT + VdP + \sum_i \mu_i dN_i. \quad (\text{A.5.4})$$

By using these definitions together with Euler's relation:

$$U = TS - PV + \sum_i \mu_i dN_i, \quad (\text{A.5.5})$$

and the second law of thermodynamics:

Substituting into expressions for the other main potentials, the following expres-

sions for the thermodynamic potentials are written as;

$$F = -PV + \sum_i \mu_i dN_i, \quad (\text{A.5.6})$$

$$H = TS + \sum_i \mu_i dN_i, \quad (\text{A.5.7})$$

$$G = \sum_i \mu_i dN_i. \quad (\text{A.5.8})$$

By using Eqs. A.5.1 and A.5.5 and $\Omega = -PV$, one can obtain

$$d\Omega = -SdT - PdV - \sum_i N_i d\mu_i. \quad (\text{A.5.9})$$

From Eq. A.5.9 the entropy S , pressure P and particle number N can be obtained from the thermodynamic potential Ω

$$S = - \left(\frac{\partial \Omega}{\partial T} \right)_{V, \mu_i}, \quad (\text{A.5.10})$$

$$P = - \left(\frac{\partial \Omega}{\partial V} \right)_{T, \mu_i}, \quad (\text{A.5.11})$$

$$N = - \left(\frac{\partial \Omega}{\partial \mu_i} \right)_{V, T}. \quad (\text{A.5.12})$$

APPENDIX B

B.6 Density of States with Magnetic Field

To investigate thermodynamic functions one should calculate DOS in a magnetic field. The kinetic energy of two dimensional electrons in \mathbf{k} space is described by

$$E_k = \frac{\hbar^2}{2m^*}(k_x^2 + k_y^2). \quad (\text{B.6.1})$$

In the ground state the electrons of the 2DES can be represented as points inside a circle in the \mathbf{k} space (Fig. B.1). The energy at the edge of the circle is called the Fermi energy E_F and given by

$$E_F = \frac{\hbar^2}{2m^*}k_F^2, \quad (\text{B.6.2})$$

with the magnitude of the wavevectors k_F at the Fermi circle. There is only one point in the area element $A = (2\pi/L_x)(2\pi/L_y)$ of the \mathbf{k} space. The number of electrons N_{el} existing in the Fermi circle is given by

$$N_{\text{el}} = \frac{2\pi k_F^2}{(2\pi/L_x)(2\pi/L_y)} = \frac{k_F^2}{2\pi}A, \quad (\text{B.6.3})$$

where the factor 2 comes from the allowed spin-up and spin-down state. Thus, the electron density of 2DES is derived

$$n_{\text{el}} = \frac{N_{\text{el}}}{A} = \frac{k_F^2}{2\pi}. \quad (\text{B.6.4})$$

Using the E_F , this equation is rewritten as

$$n_{\text{el}} = \frac{m^*}{\hbar^2 \pi} E_F. \quad (\text{B.6.5})$$

This equation gives two important knowledge; (i) the electron density is independent of temperature, (ii) the Fermi energy decreases to keep the number of electrons in the system constant.

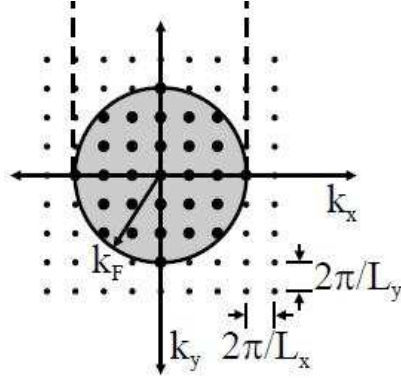


Figure B.1 A schematic diagram represents the Fermi circle. The points symbolize the two dimensional electrons in the \mathbf{k} space.

Another very important characteristic of the 2DES is the density of states $D(E)$ that describes the distribution of energies

$$\begin{aligned}
 D(E) &= \frac{\partial n_{\text{el}}}{\partial E} = \frac{\partial}{\partial E} \left[\frac{m^*}{\hbar^2 \pi} E_n \right] \\
 &= \frac{\partial}{\partial E} \left[\frac{m^*}{\hbar^2 \pi} \hbar \omega_c \left(n + \frac{1}{2} \right) \right] \\
 &= \frac{eB}{\hbar \pi} \sum_{n=0}^{\infty} \delta(E - E_n). \tag{B.6.6}
 \end{aligned}$$

By substituting magnetic length $l = \sqrt{\hbar/(eB)}$ into this equation, DOS is obtained as

$$D(E) = \frac{g_s}{2\pi l^2} \sum_{n=0}^{\infty} \delta(E - E_n), \tag{B.6.7}$$

with degeneracy factor g_s . According to the DOS, the electron density can be obtained.

$$n_{\text{el}} = \int dE f(E) D(E). \tag{B.6.8}$$

Here $f(E)$ is the Fermi function and given by

$$f(E, \mu, T) = \frac{1}{\exp\left[\frac{(E-\mu)}{k_B T}\right] + 1}.$$

Using $\int f(E)\delta(E - E_n)dE = f(E_n)$, the electron density is found as

$$\begin{aligned} n_{\text{el}}(E, \mu, T) &= \frac{g_s}{2\pi l^2} \int d(E)f(E) \sum_{n=0}^{\infty} \delta(E - E_n) \\ &= \frac{g_s}{2\pi l^2} \sum_{n=0}^{\infty} f(E_n). \end{aligned} \quad (\text{B.6.9})$$

Eq. B.6.9 shows that electron density can be written as a function of the temperature. Thus, DOS should also depend on temperature.

$$\begin{aligned} D(E, \mu, T) &= \frac{dn_{\text{el}}}{d\mu} = \frac{g_s}{2\pi l^2} \frac{d}{d\mu} \left[\sum_{n=0}^{\infty} f(E_n) \right] \\ &= \sum_{n=0}^{\infty} \frac{g_s}{2\pi l^2} \frac{d}{d\mu} [f(E_n)] \\ &= \sum_{n=0}^{\infty} \frac{g_s}{2\pi l^2} \frac{d}{d\mu} \left[\frac{1}{\exp\left(\frac{(E_n - \mu)}{k_B T}\right) + 1} \right] \\ &= \sum_{n=0}^{\infty} \frac{g_s}{2\pi l^2} \left[\underbrace{\exp\left(\frac{(E_n - \mu)}{k_B T}\right) + 1}_{(1/f(E_n))^{-2}} \right]^2 \left[\underbrace{\frac{1}{k_B T} \exp\left(\frac{(E_n - \mu)}{k_B T}\right)}_{(1-f(E_n))/f(E_n)} \right] \\ &= \sum_{n=0}^{\infty} \frac{g_s}{2\pi l^2} f(E_n)^2 \left(\frac{1 - f(E_n)}{f(E_n)} \right) \\ &= \sum_{n=0}^{\infty} \frac{g_s}{2\pi l^2} \frac{1}{k_B T} f(E_n) [1 - f(E_n)] \end{aligned} \quad (\text{B.6.10})$$

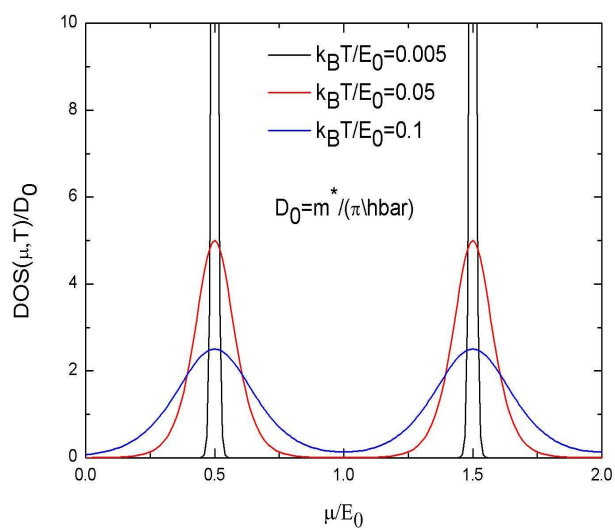


Figure B.2 Density of states for different values of temperature with fixed magnetic field.

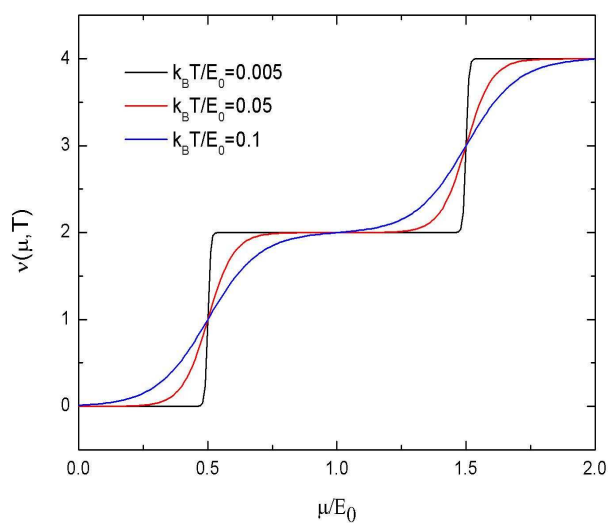


Figure B.3 Electron density profile versus for different values of temperature with fixed magnetic field.

ABBREVIATIONS and SYMBOLS

| | |
|---|--|
| 2DES | Two-dimensional electron system. |
| $2d$ | Sample width. |
| B | Magnetic field. |
| b | Depletion length. |
| DOS | Density of states. |
| ε_α | energy of the α -th Landau level without the potential. |
| e | Electron charge. |
| $E_{\text{bg}}^0 = 2\pi e^2 n_0 d / \bar{\kappa}$ | Pinch-off energy. |
| E_{F}^0 | Fermi energy at the center. |
| Γ_L | Landau level broadening. |
| h | Planck's constant. |
| IQHE | Integer Quantum Hall effect. |
| IS(s) | Incompressible strip(s). |
| $j_{n_{\text{el}}}$ | number flux density. |
| j_q | Thermal flux density. |
| κ | Dielectric constant. |
| k_{B} | Boltzmann's constant. |
| $\ell = \sqrt{\hbar/m^* \omega_c}$ | Magnetic length. |
| LL(s) | Landau level(s). |
| m^* | Effective electron mass. |
| μ | Chemical potential. |
| μ_{ec} | Electrochemical potential. |
| ν | Filling factor. |
| $\nu(0)$ | Filling factor at the center. |
| n_0 | Donor density. |
| n_{el} | Electron density. |
| P_L | energy loss. |

| | |
|---------------------------------|-------------------------------------|
| QHE | Quantum Hall effect. |
| QHS | Quantum Hall system. |
| TFA | Thomas-Fermi approximation. |
| TFPA | Thomas-Fermi-Poisson approximation. |
| T_L | Lattice temperature. |
| T_{el} | Electron temperature. |
| $\omega_c = eB/mc$ | Cyclotron frequency. |
| $\Omega_c \equiv \hbar\omega_c$ | Cyclotron energy. |
| \mathbf{v}_D | Drift velocity. |
| V_{bg} | Background potential energy. |
| V_H | Hartree potential energy. |